Int. J. Electrochem. Sci., 3 **(2008)** 1463 - 1503

International Journal of ELECTROCHEMICAL SCIENCE
www.electrochemsci.org

The Oxygen Evolution Reaction on Passive Oxide Covered Transition Metal Electrodes in Alkaline Solution. Part III – Iron.

Michael E. G Lyons[*], *Michael P Brandon*

Physical and Materials Electrochemistry Laboratory, University of Dublin, Trinity College, Dublin 2, Ireland
[*]E-mail: melyons@tcd.ie

Received: 24 October 2008 / *Accepted:* 6 November 2008 / *Published:* 17 November 2008

The kinetics of the oxygen evolution reaction (OER) at passive oxide covered polycrystalline Fe electrodes in aqueous alkaline solution were examined using both dc steady state polarisation and ac impedance techniques. It proved difficult to obtain reproducible polarisation data for bright anodes, and so an electrochemical pre-treatment routine was devised. Upon ageing of a given electrode specimen, and with application of the pre-treatment regime before each experiment, it was possible to determine reproducible values of the Tafel slope and the reaction order with respect to OH^- ion activity. The link between OER polarisation behaviour and the changing nature of the passive oxide film, with repeated electrode pre-treatment and experimental utilisation, was characterised by cyclic voltammetry. As was previously found for oxidised Co electrodes, it is necessary to admit a dual energy barrier model in order to rationalise some of the experimental Tafel slope values. By considering the kinetic data presented here, in tandem with complimentary results obtained for extensively aged and also for multicycled iron electrodes, a preferred reaction pathway emerges. The electrode active surface area for the OER has been been estimated using the same current transient decay technique that we have applied to Ni and Co anodes. On this basis, the "real" surface area normalised activity series for the OER amongst the passive oxides of these first row transition metals is outlined.

Keywords: oxygen evolution electrocatalysis, oxidized iron electrodes, transition metal electrochemistry, oxygen evolution mechanisms

1. INTRODUCTION

The present article is the concluding instalment of a three part series, the previous parts of which, have considered the oxygen evolution reaction (OER) at passive oxide covered polycrystalline

Ni [1] and Co [2] electrodes in aqueous alkaline solution. The motivations behind this body of work were outlined in the first paper of the series [1].

The oxygen evolution electrocatalytic properties of oxidised Ni electrodes have received much attention in the literature [1], while several independent workers have investigated the details of the reaction at oxidised Co anodes [2]. By contrast, to the best of our knowledge, the only meaningful studies of the kinetics of the OER at oxidised Fe substrates are those of the present authors [3,4] and a rather limited early contribution by Scarr [5]. Our preliminary communication [3] on this matter dealt primarily with the OER electrocatalytic properties of relatively thick polymeric hydrous oxide films generated by the repetitive potential cycling of an iron electrode in alkaline solution. Tafel slopes of $b \approx 2.303(RT/F)$ (≈ 60 mV dec^{-1} at 25ºC) and $b \approx 2.303(2RT/F)$ (≈ 120 mV dec^{-1} at 25ºC) were observed for such electrodes in 1.0 M NaOH solution, at lower and higher oxygen overpotentials respectively. On this basis a possible OER pathway was outlined, that was in essence a modification of the classic mechanism of Krasil'shchikov [6], which is in turn, probably the most commonly cited oxygen evolution pathway for oxide electrodes in the literature.

We have revisited this system more recently [4] – in addition to confirming the Tafel slope parameters detailed above, experimental values of the reaction order with respect to OH^- ion activity, m_{OH^-}, were determined by conducting OER steady state polarisation experiments in NaOH solutions of different concentrations. These measurements indicated that a non-integral reaction order of ca. 3/2 is associated with the ~60 mV dec^{-1} Tafel region, while an order of approximately unity characterises the higher overpotential straight line Tafel region. Similar experimental values of b and m_{OH^-} were obtained for pre-reduced, "aged", passive oxide covered Fe anodes [4] – i.e. aged electrodes which were not subjected to potential multi-cycling to deliberately deposit a hydrous oxide phase. Of course, bright iron electrodes spontaneously become passivated upon introduction to an aqueous alkaline solution [7] and the passive oxide is further developed by anodic polarisation [4, 8], with the result that oxygen evolution will always occur at an *oxidised* iron surface, regardless of whether or not, an oxide has been deliberately grown prior to the OER steady state polarisation experiment. In the case of the "aged" passive oxide covered Fe electrodes mentioned above, reproducibility in OER experiments was ensured by a single prior voltammetric cycle (note, that the electrodes were cathodically pre-reduced before this) [4].

The possession of a more complete kinetic data set (now with well defined m_{OH^-} values in addition to the b values) forced a revision in our viewpoint regarding the most likely pathway for the OER at the aforementioned "types" of oxidised iron electrodes [4] – the modified Krasil'shchikov pathway was rejected in favour of the so-called physisorbed hydrogen peroxide mechanism:

$$S + OH^- \rightarrow S - OH + e^- \quad \text{(AI)}$$

$$S - OH + OH^- \rightarrow S - H_2O_2 + e^- \quad \text{(AII)}$$

$$S - H_2O_2 + OH^- \rightarrow S - HO_2^- + H_2O \quad \text{(AIII)}$$

$$S - H_2O_2 + S - HO_2^- \rightarrow O_2(g) + H_2O + OH^- \quad \text{(AIV)}$$

In the above scheme S represents an electrocatalytically active site on the oxide surface, while S- -H_2O_2 represents *physisorbed* hydrogen peroxide. This type of mechanism was first devised by

Bockris and Otagawa [9] to describe the OER at perovskite electrode substrates, and is, to the best of our knowledge, uniquely capable, amongst the various OER paths that have been postulated in the literature [9 – 11], of rationalising the set of experimental kinetic parameters that we have observed for multi-cycled and "aged" passive Fe electrodes. The lower overpotential polarisation behaviour is explained, by considering (A II) to be the rate determining step (RDS) under Temkin adsorption conditions (i.e. $0.2 \leq \theta \leq 0.8$, where θ is the fractional coverage of OER intermediate species). The experimental values of b and m_{OH^-} obtained at higher overpotentials arise from a conventional kinetic analysis if (A II) is again taken as the RDS, this time under high coverage Langmuir adsorption conditions (i.e. $\theta \rightarrow 1$). We have outlined elsewhere [4] the kinetic analysis for the two aforementioned situations in full, as well as discussing the requirement for the formation of a physisorbed, as opposed to chemisorbed, intermediate species in the rate limiting second step. In addition, on the basis of our own voltammetric data, and with reference to some literature sources, we have tentatively suggested [4] that S is an Fe(VI) based entity, stabilised at high anodic potentials on the surface of the outer dispersed and hydrous oxide phases that are likely to exist for both multi-cycled and "aged" iron electrodes in aqueous alkaline media.

In the present article it will be shown that OER polarisation measurements on relatively un-aged, passive oxide covered Fe electrodes, yield different values of b and m_{OH^-} to those outlined above for more aged and for muti-cycled anodes. Despite this it will be shown, in a manner consistent with our interpretation of the OER kinetic data for oxidised Ni [1] and Co [2] electrodes, that a slight modification of scheme (A) can provide a satisfactory rationalisation for each of the sets of experimental parameters (b and associated m_{OH^-}) that we have encountered for the various "types" of oxidised Fe electrodes that we have studied.

Following the mechanistic analysis, a series of current transient decay measurements will be outlined, which were aimed at the estimation of the active surface area of the passive oxide covered Fe electrodes towards the OER, based upon the technique originally described by Ho and Piron [12]. This surface roughness factor estimation technique was also applied to passive oxide covered Ni [1] and Co [2] OER electrodes, thereby enabling us to make a meaningful comparison of the catalytic activities of the passive oxides of the three metals for the OER, based upon the active surface area normalised current density values at a given overpotential.

At the end of the article, we outline our principal conclusions regarding the OER at passive oxide covered, first row transition metal electrodes, based upon the results detailed across the three papers of the series. We believe that these conclusions are worthy of consideration by workers involved in the wider science of OER anodic materials research, particularly since some of the more practically promising materials are oxides and mixed oxides (i.e. spinels or perovskites) of Ni and Co.

2. EXPERIMENTAL PART

2.1. Materials and methods

The experimental details are similar to those described in the previous instalments of this series [1, 2] and so we restrict ourselves here to a brief overview. A standard three electrode cell arrangement

was utilised. The electrochemical measurements were all performed using a Zahner Elektrik IM6 Impedance measurement unit (with its in-built frequency response analyser (FRA) for electrochemical impedance spectroscopy (EIS) measurements) interfaced to a personal computer. The SIM module of the IM6 Thales software suite facilitated *complex non-linear least squares* (CNLS) fitting of raw EIS data to equivalent circuit models. Consistency between the measured values of impedance magnitude $|Z|$ and phase angle were checked using the *Kramers-Kronig rule check* option provided by the Thales software package – any data failing this test were rejected.

All electrolyte solutions were prepared from NaOH pellets (BDH AnalaR®, minimum 98% purity) using millipore water (resistivity > 18 MΩcm). No excess salts were added and all experiments were conducted at 25 ± 1°C. The OH^- activity, a_{OH}, for each solution concentration was calculated using the literature value [13] for the mean ionic activity coefficient, $\gamma_{\pm}$, for an NaOH solution of that concentration. Electrode roughness factors were estimated using the OH_{ads} desorption method of Ho and Piron [12] – a schematic diagram of the appartus for such measurements was included in the first article of this series [1].

2.2. Electrode preparation and pre-treatment

The iron electrodes were prepared from a 1mm thick polycrystalline iron foil as supplied by Alfa Aesar (Johnson Matthey), purity 99.995% (metals basis). Sections of the foil were cut and filed to a size of 4 mm × 4 mm (exposed geometric surface area = 0.16 cm^2), and were then sealed into glass tubes in an identical manner to that described elsewhere[1] for the preparation of Ni electrodes. Before its first experimental use, the exposed metal surface was polished successively with 1200 grit carbimet paper and a slurry of 0.05 micron alumina powder (in millipore water) until a "mirror bright" finish was achieved.

As in our communications on the OER at oxidised Ni [1] and Co [2] anodes, it is useful at this stage to distinguish between the various "types" of Fe electrode investigated in the present work. These electrodes are, of course, all just passivated iron, however their OER electrocatalytic properties vary somewhat as a result of differences in pre-treatment or polarisation history. For clarity we will refer to Fe electrodes "types" A – C, where:

- Type A: A bright electrode was polished in a slurry of 0.05 micron alumina powder, rinsed in de-ionised water and used directly in this condition.
- Type B : A bright electrode was polished as for A, but was then *pre-reduced* in 1.0 M NaOH solution at a potential of –1.1 V (vs. Hg/HgO) for a period of 5 minutes. Following this, the electrode was allowed to rest on open circuit for 10 minutes. The pre-treatment was completed by one potentiodynamic cycle between the limits of –1.175 and 0.625 V in the same 1.0 M NaOH solution, at a scan rate of 40 mV s^{-1}.
- Type C: This is a somewhat aged "type" B anode.

In the results section it will be shown that even when subjected to pre-treatment B before each experiment, the OER steady state polarisation behaviour of a *freshly prepared* iron anode displays

some variability over the course of its first number of polarisation experiments. As will be outlined later, stability was observed after approximately 10 experiments – and it is this stabilised pre-reduced Fe electrode that will be referred to as a "type" C electrode. It is important to note that, prior to each polarisation experiment, the electrode was still subjected to pre-treatment routine B.The reader should also avoid confusing this relatively mildly aged electrode (Type C) with the "aged" Fe electrode mentioned to in the introduction and described elsewhere [4]. The latter refers to an iron electrode that was used in many polarisation experiments (> 40 over the course of four months) and its OER catalytic behaviour is characterised by different values of b and m_{OH^-} than were observed (results section) for the "type" C anode under investigation in the present article.

2.3. Reference and counter eletrodes

A mercuric-mercuric oxide reference electrode (Radiometer Analytical, cat no. XR400) was used throughout the present study. As we have previously discussed [1], the equilibrium oxygen electrode potential is is 0.303 V vs. Hg/HgO in the same solution. It is common practice in the literature [14-16] on the OER, to express potential in terms of the oxygen overpotential, η, when the reference electrode is a Hg/HgO electrode in the same solution as the working anode. In this case η is related to the voltage E_{meas} measured on the Hg/HgO scale (at a temperature of 298 K) as follows:

$$\eta = E_{meas} - 0.303\,V \tag{1}$$

For the sake of consistency it was elected to use Hg/HgO, 1M NaOH, throughout the present study. It is therefore appropriate to plot polarisation curves on an oxygen overpotential, η, scale, in cases where all the data has been recorded in 1.0 M NaOH solution. This approach is useful for comparing the OER catalytic performance of an electrode, with that of other anodes reported in the literature.

When used in NaOH solutions of different concentrations, the potential of the Hg/HgO electrode was checked relative to a second Hg/HgO, 1 M NaOH electode, both before and after the experiment. No significant potential drift was noted after such experiments, implying that the concentration of the NaOH in the reference electrode chamber remains effectively constant over the time scale of typical polarisation measurements (ca. 2 – 3 hours). In any case, the 1M NaOH solution in the reference electrode, was changed regularly to ensure experimental consistency. Graphs containing data recorded in electrolyte solutions other than 1.0M NaOH, are plotted in terms of the potential, E, vs. Hg/HgO, 1M NaOH.

Finally it is noted that a platinum wire electrode (CH Instruments, Inc. -catalogue no. CHI 115) was employed as the counter electrode.

3. RESULTS AND DISCUSSION

3.1. Review of the surface electrochemistry of Fe electrodes in aqueous alkaline solution

The close interrelationship between the surface redox chemistry of transition metal electrodes and their steady state oxygen evolution polarisation behaviour has been emphasised in the previous instalments of this series, and accordingly it was considered pertinant to provide brief reviews of the aqueous alkaline electrochemistry of Ni [1] and Co [2] electodes before discussing their electrocatalytic activites for the OER. In the case of Fe, we have already discussed the surface oxide and oxyhydroxide electrochemistry in detail some years ago [8] and recently in a more succinct form [4]. We therefore provide a very brief overview of the topic below, and refer the reader who seeks a greater level of detail to our aforementioned earlier works and those of other authors [4, 17 – 23].

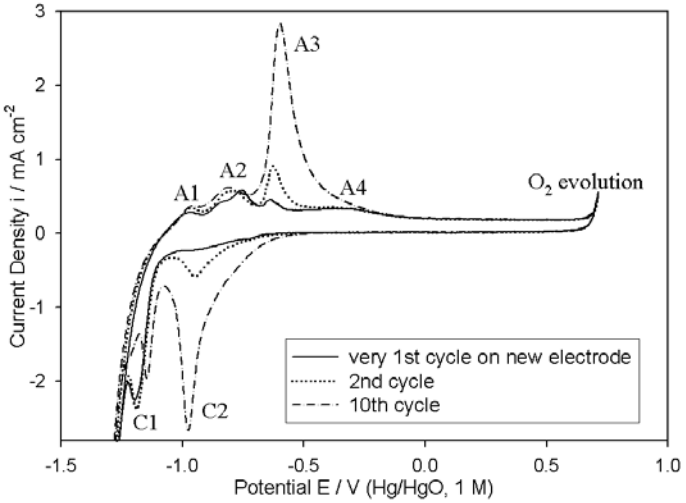

Figure 1. 1st, 2nd and 10th voltammetric cycles (-1.42 V to 0.68 V, 40 mV s^{-1}) for a "type" A iron electrode in 1M NaOH at 25°C.

Voltammetric studies have provided considerable insight into the passivation of metallic Fe – in Fig. 1 a series of cyclic voltammograms, recorded for a freshly prepared bright iron electrode in 1.0 M NaOH solution, are reproduced from our recent article [4]. As was discussed in that communication, the profile of the 2nd cycle of Fig. 1 is more similar in form to that normally observed voltammetrically following the polishing back to a bright finish, of a previously passivated iron electrode. The 1st cycle of Fig. 1 was only observed for a previously unused electrode. This points to a common theme in the present series [1, 2, 4] – namely the gradual ageing of first row transition metal electrodes by the the build up, over time (while the electrode is repeatedly used in anodic experiments), of a residual oxide phase that is resistant to removal by normal mechanical polishing (i.e. with slurrys of alumina). As already noted [1, 2, 4], such ageing occurs despite careful polishing and rinsing of electrodes prior to, and after polarisation experiments. The differences in profile between the 1st cycle of Fig. 1 for an unused electrode and all subsequent scans for the same electrode when it had been polished "bright" after passivation [4], point to the development of a thin, strongly bound(and not readily removable) oxide layer immediately adjacent to the metal surface. We have also speculated [2] that residual oxide development will be faciliated by microscale scratching (surface roughness) of the metallic surface creating areas where oxide can grow, but which are effectively inaccessible to the rather "blunt instrument" of alumina polishing. Whatever the location and nature of the residual oxide, it will be

shown in the present paper that electrode ageing provides an even greater obstacle to the attainment of reproducible OER polarisation data in the case of Fe electrodes, than it did for Ni [1] or Co [2]anodes.

It is evident from Fig. 1 that upon repetitive potential cycling, the redox charge capacity *Q* (as estimated by integration of the voltammetric profile between appropriate limits) is enhanced only for the A3 and C2 peaks. Indeed, we have previously reported [8] that, while the other peaks exhibit zero shift in peak potential with respect to a pH independent reference electrode over a range of solution pH (~7-14), the complimentary peaks A3 and C2 display a *super-Nerstian shift* of the order of $\frac{dE}{dpH} = -\frac{3}{2}\left(2.303\frac{RT}{F}\right)$ V/pH unit with increasing pH. Such super-nernstian shifts are characteristic of electrochemically generated hydrous oxide phases [24].

Bearing in mind the observations of the foregoing paragraph, we have made the following peak assignments [4, 8] in relation to the voltammetric data of Fig. 1. Peak A1 is most probably due to the formation of a layer of adsorbed hydroxyl species,

$$Fe + OH^- \rightarrow FeOH(ads) + e^- \tag{2}$$

In combination with a displacement of adsorbed hydrogen:

$$FeH(ads) \rightarrow Fe + H^+ + e^- \tag{3}$$

In agreement with other workers [17 – 21], we have proposed [8] that peak A3 is associated with the formation of ferric species, however we have postulated, based on the aforementioned super-nerstian shifts, that the operative reaction is not the formation of species such as Fe_2O_3 or FeOOH in a compact well defined phase, but rather a Fe(II)/Fe(III) transition in an *outer dispersed hydrous* oxide phase. Such a phase is envisaged to result from the hydration and oxidation of the external surface region of the Fe(II) oxides formed in eqns. 4 and 5. The oxide is thus envisaged to take on a dual layer structure [4] in line with a model proposed some time ago by Burke et al.[25 – 27] These workers proposed that for some transition metals (e.g. Ir, Rh and Ni) the anodic oxide comprises an inner compact anhydrous layer MO_x and an outer microdispersed hydrous layer of general form $MO_a(OH)_b(OH_2)_c$.

The decrease in the peak potential of A3 (and indeed its complimentary cathodic peak C2) with increasing pH points to the formation of an anionic hydrous oxyhydroxide species. We have proposed [4] that the complex redox switching process, which forms the outer dispersed hydrous oxide by the oxidation of the hydrated surface region of the Fe(II) based oxide may be written as:

$$\left[Fe_2(OH)_6(OH_2)_3\right]^{2-} + 3OH^- \rightarrow \left[Fe_2O_3(OH)_3(OH_2)_3\right]^{3-} + 3H_2O + 2e^- \tag{6}$$

An equivalent representation, which emphasises the anionic nature of the outer region of the oxide in aqueous alkaline solution, is given by:

$$Fe(OH)_2 \cdot nH_2O + 0.5Na^+ + 1.5OH^- \rightarrow \left[Fe(OH)_{3.5} \cdot nH_2O\right]^{0.5-} \cdot \left(Na^+\right)_{0.5} + e^- \tag{7}$$

Peak A4 is also related to an Fe(II)/Fe(III) redox transition – however at this potential it is the inner amorphous region of the Fe(II) oxide, close to the metal surface, that is oxidised. Possibly oxidation products are largely anhydrous phases of Fe_2O_3, Fe_3O_4 or FeOOH. The cathodic C1 peak, is in turn related to the reduction of this inner compact layer back to metallic iron. The increasing redox charge associated with the A3/C2 peak pair upon multi-cycling, indicates the importance of the redox switching process in the outer hydrous layer (i.e. that represented by eqn. 6) with regard to the growth of thick multi-cycled oxide phases [4, 8]. In the present article we are more concerned about the initial passivation of Fe electrodes, however the presence of the A3 and C2 peak features in the profile of the 2nd voltammetric cycle of Fig. 1 (recall from earlier this is typical of the 1st cycle of electrodes that have been polished back to a "bright" finish following previous passivation) and indeed in the voltammograms of Fig. 5 indicate that the dual layer nature of the anodic oxide formed on iron is significant from the very beginning of passivation under conditions of anodic polarisation in alkaline media.

In the voltammetric characterisation of passive oxide covered Ni and Co electrodes, it was observed that the rising edge of the OER current density appeared directly anodic to the Ni(II)→Ni(III) oxidation peak in the case of Ni anodes [1], and, for Co electrodes [2], developed from the anodic feature associated with the surface oxidation of Co(III)→Co(IV) species. We therefore concluded (in tandem with some other considerations) that oxygen evolution is most likely catalysed by Ni(III) and Co(IV) entities respectively for oxidised electrodes of these metals. Referring to Fig. 1, it is obvious that the anodic redox peak (A4) closest in potential to the onset of the oxygen evolution current feature, is separated from the latter by approximately ¾ of a volt! This absence of an obvious "preceeding redox transition" in the case of oxygen evolution on oxidised iron, raises questions as to the valance state of the OER electrocatalytic entity for this substrate. As alluded to in the Introduction, we have suggested that the aforementioned active sites are Fe(VI) species. The experimental results on which this hypothesis is based, and the reason why the Fe(III)↔Fe(VI) redox transition is not normally sensitive to detection by voltammetry, have been discussed in detail elsewhere [4].

3.2. Steady state polarization measurements: Fe electrode' type' A

A series of *iR* compensated OER steady state polarisation curves for a "type" A Fe electrode in various NaOH solutions are presented in Fig. 2. These measurements were conducted on successive days (one experiment per day) in the order indicated in the legend. From the point of view of extracting meaningful values of the reaction order parameter m_{OH^-}, several difficulties arise with the data of Fig. 1. Firstly, a lack of coincidence is noted between the two 1.0 M traces. It is obvious that the OER electrocatalytic activity of the electrode has diminished between the earlier and later 1.0 M experiments, even though these were separated by just two days. In the intervening period the 0.5 M polarisation curve was recorded, and the electrode was polished to a mirror bright finish, before and after each measurement. Decreases in OER activity were also noted when 0.5 and 1.0 M experiments were repeated, after the completion of the measurements detailed in Fig. 1, although, just as with the 1.0 M curves of that figure, it was observed that the Tafel slope remained essentially constant. It would

therefore appear, that it is extremely difficult to record reproducible oxygen evolution polarisation data for bright Fe anodes, probably due to electrode ageing effects related to the inability of polishing alone, to completely remove the oxide formed during anodisation, as discussed in the review above on iron oxyhydroxide electrochemistry. Similar problems were noted for bright Ni anodes [1], although in that case we postulated that it was a variation, with ageing, of the relative amounts of the active oxide existing in the β-β or α-γ Bode cycles, that mainly caused the irreproducibility in OER polarisation measurements. By contrast, the polarisation behaviour of bright Co electrodes displayed satisfactory reproducibility, over the course of a number (~10) of successive experiments [2].

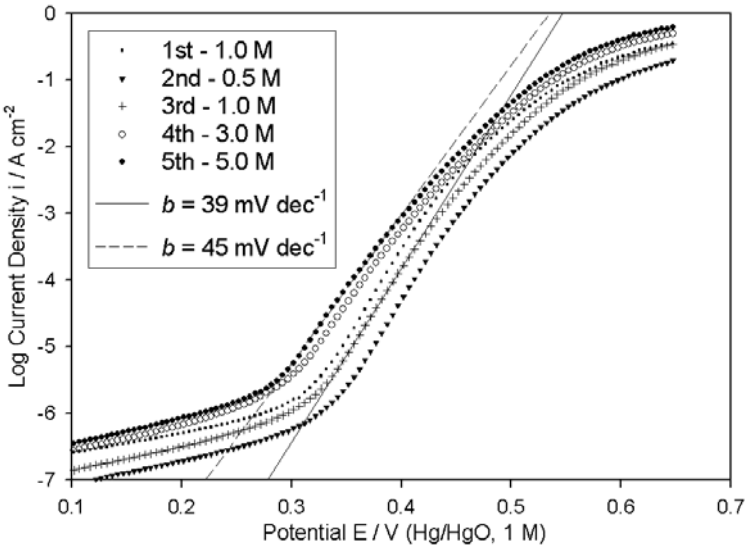

Figure 2. *iR* corrected, OER steady state polarisation curves measured in the direction of increasing potential for a "type" A iron electrode in NaOH solutions of various concentration. These characteristics were recorded on consecutive days in the order indicated in the legend.

A further difficulty is that the value of the Tafel slope in the lower overpotential region increases progressively with increasing OH^- concentration, from 39 mV dec^{-1} ($\cong 2.303(2RT/3F)$ at 25ºC) for 0.5 and 1.0 M electrolyte to 45 mV dec^{-1} ($\cong 2.303(4RT/5F)$ at 25ºC) for 5.0 M NaOH solution. The possibility was considered that this observation was an artifact arising from electrode ageing (remember that the 5.0 M data was the last to be recorded) – however the measured values of *b* for each solution remained the same when the polarisation experiments were repeated in the opposite order. A somewhat similar phenomenon was observed [2] for OER polarisation measurements performed with bright (non-electrochemically pre-treated) Co electrodes, although in that case the directly opposite trend prevailed – i.e. the Tafel slope decreased from $b \cong 2.303(4RT/5F)$ for 1.0 M NaOH to $b \cong 2.303(2RT/3F)$ for 5.0 M NaOH.

Previously [1, 2] each of the aforementioned problems were circumvented for the respective electrodes (i.e. irreproducibility in the case of Ni, and variation in *b* with $[OH^-]$ for Co) by applying

electrochemical pre-reduction routines and consequently it was decided that a similar approach was necessary in the present case.

3.3. Steady state polarization measurements : Fe electrode' type' B

A bi-directional oxygen evolution steady state polarisation curve, recorded in 1.0 M NaOH for an Fe electrode that had been subjected to pre-treatment routine B, as outlined in the Experimental section, is presented in Fig. 3. As we previously noted for oxidised Ni [1] and Co [2] electrodes there is significant hysterisis between the log $i(\eta)$ characteristic recorded in the direction of increasing potential (forward) and that of the direction of decreasing potential (reverse). Such hysterisis was also observed for A and C "type" Fe anodes.

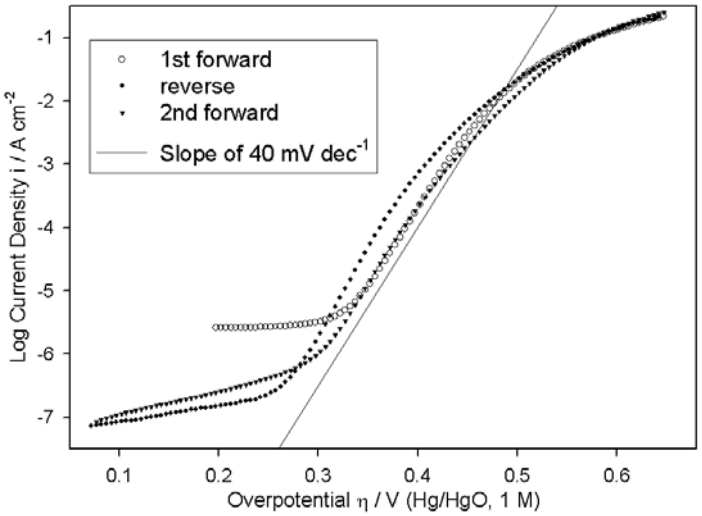

Figure 3. Bi-directional, *iR* corrected, OER steady state polarisation curve for a "type" B iron electrode in 1.0 M NaOH at 25°C. This data was recorded continuously, started in the direction of increasing potential.

In the case of Ni and Co OER electrodes, the scans in opposing directions were largely coincident at potentials associated with the lower straight line Tafel region, while at higher overpotentials the reverse direction sweeps were characterized by lower values of log i at a given η than were prior sweeps recorded in the direction of increasing potential. The issue of hysterisis in OER steady state polarisation characteristics has received very little attention in the literature, with the majority of authors detailing measurements recorded in one direction only. A notable exception in this regard are Kobussen et al., who reported hysterisis of a similar nature to that described above for Ni and Co anodes, in OER studies at both $La_{0.5}Ba_{0.5}CoO_3$ [28] and polycrystalline Co [14] electrodes in alkaline solution. In the $La_{0.5}Ba_{0.5}CoO_3$ case they attributed the decrease in activity on a reverse direction sweep, relative to a prior forward direction scan, to a conversion of OER active Co(III) surface sites into inactive Co(IV) sites at extreme anodic overpotentials [29]. This explanation is

however inconsistent with our viewpoint [2] that it is Co(IV) entities that are electrocatalytically active for the OER. The hysterisis effect might instead be understood in terms of a decrease in the conductivity of the underlying oxide phase accompanying polarisation at high overpotentials, arising either from film thickening or due to a change in the nature of the oxide (related possibly to dehydration at extreme potentials).

Whatever the origin of the aforementioned effects for Ni, Co and $La_{0.5}Ba_{0.5}CoO_3$ anodes, it is apparent from Fig. 3, that the hysterisis in oxidised Fe OER polarisation curves is entirely different. In this case the the reverse direction scan displays superior OER activity relative to the prior forward scan, over a range of overpotentials from ca. 335 mV to ca. 500 mV. In addition the slope of the straight line Tafel region on the reverse sweep is slightly less (~36 mV dec^{-1}) than that observed for the forward sweeps (~40 mV dec^{-1}). The indication here is, that for oxidised iron electrodes, polarisation at extreme anodic potentials either produces a greater surface density of the Fe(VI) OER electrocatalytic entity or alternatively reduces the resistivity of the passive oxide.

It should be noted that the type of hysterisis described above for Fe electrodes also prevails when the reverse direction sweep is performed first (following stabilsation of the current density at a high overpotential) with the subsequent (and continuous) recording of the scan in the direction of increasing potential. However, while satisfactory reproducibility in OER steady state measurements was finally achieved for pre-reduced electrodes with the first polarisation sweep in the forward direction (as will be described presently), it couldn't be achieved for the case of pre-oxidation followed by polarisation in the direction of decreasing potential. The latter approach was successfully adopted for the measurement of OER polarisation curves at Pt electrodes by Damjanovic et al. [30-32], but given the intrinsic differences in the anodic oxidation mechanism of Pt compared to base metals such as Fe [7], it is not surprising that it is much more difficult to restore an Fe electrode to a pre-polarisation state (by electrochemical reduction and polishing) than is the case for Pt.

In view of the comments of the two foregoing paragraphs, the experimental values of b and m_{OH^-} considered in this article have been extracted from the first steady state polarisation sweep in the direction of increasing potential for each of the "types" of Fe electrode. This approach is consistent with the methodology adopted in the prior instalments of this series [1, 2], the reasoning behind which, has been discussed previously [1].

While it was possible to record reproducible OER steady state polarisation curves similar to that of Fig. 3 for the first three or four polarisation experiments (each conducted following the application of pre-treatment procedure B), on a freshly prepared Fe electrode, it was noted that subsequent to the fifth experimental run the values of the Tafel slope began to increase by several mV dec^{-1}. After approximately 10 polarisation measurements the Tafel slope behaviour had stabilised sufficiently to allow a reliable series of polarisation curves at different OH^- concentrations to be recorded – it is at this stage in its experimental service life that a "type" B electrode "becomes" a "type" C electrode – recall Experimental section. A comparison of OER polarisation curves in 1.0 M NaOH, recorded early in the life cycle of a pre-reduced electrode (5^{th} polarisation measurement –i.e. still "type" B), and at the stage by which the Tafel slope behaviour had stabilised (16^{th} polarisation measurement – now "type" C), is presented in Fig. 4. While a Tafel slope of 39 mV dec^{-1} was observed for the "type" B electrode, this value increased by ca. 5 mV dec^{-1} upon ageing of the electrode. Thus,

while the electrode was subjected, before each polarisation measurement, to the pre-reduction regime outlined above, and was polished thoroughly subsequent to each experiment, it appears that an ageing process was still able to influence its electrocatalytic properties towards the OER – c.f. the above review of the electrochemistry of Fe electodes.

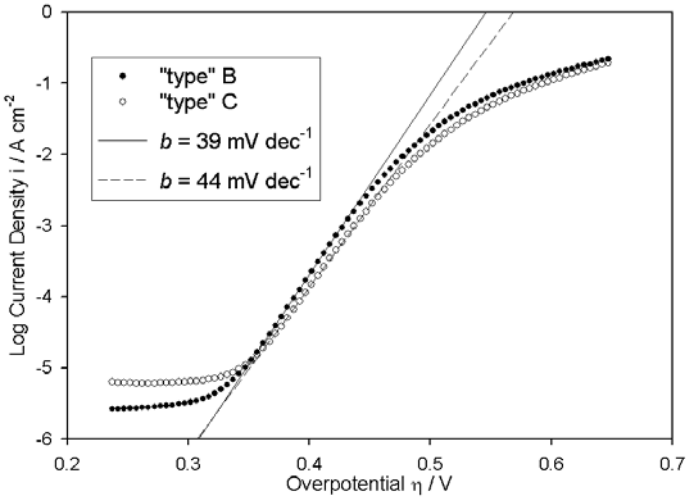

Figure 4. Comparison of *iR* corrected steady state polarisation curves, recorded in the direction of increasing potential in 1.0 M NaOH, for "type" B and "type" C iron electrodes.

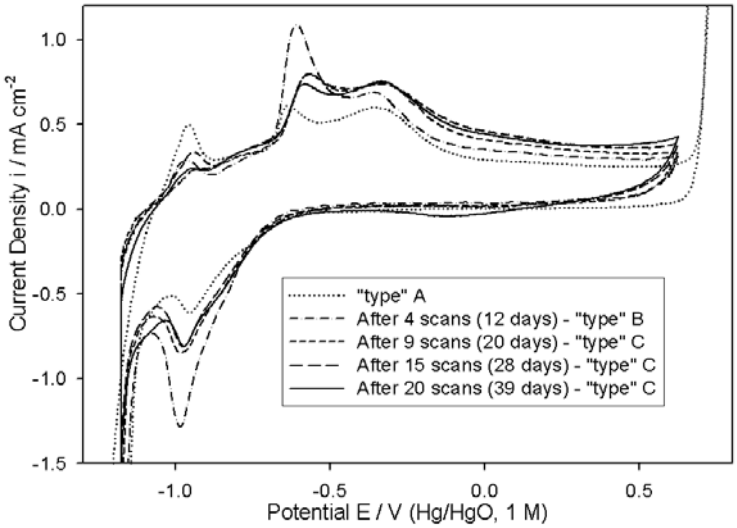

Figure 5. Cyclic voltammograms (1 M NaOH with scan rate of 40 mV s^{-1}) characterising the changing nature, with electrochemical ageing, of the passive oxide film formed on a polycrystalline Fe electrode surface. All CVs, except that of the "type" A electrode, were recorded immediately following pre-reduction of the electrode at –1.1 V for 5 minutes in the same 1 M NaOH solution.

An examination of the cyclic voltammetry profiles (CVs) recorded as the final step of the pre-reduction procedure casts some light on possible reasons for the observed increase in Tafel slope with

electrode ageing – see Fig. 5. This figure shows the development of the CV profile of a Fe electrode specimen from its initial characterisation after preparation ("type" A), to the stage at which it has become well aged, after 20 steady state polarisation experiments in NaOH solutions of various concentrations, over a period of 39 days. The "type" B polarisation curve of Fig. 4 was recorded for the electrode characterised by the "after 4 scans" profile of Fig. 5.

It can be appreciated that the CV profiles become largely similar from that recorded after 9 scans onward. This stabilisation of the CV after pre-reduction, corresponded to the stabilisation of the Tafel slopes observed in subsequent 1.0 M steady state polarisation measurements, to values of the order of 5 – 7 $mVdec^{-1}$ greater than those observed in the initial experiments on the pre-reduced electrode. Accordingly, the "type" C polarisation curve of Fig. 4 was recorded for the electrode characterised by the "After 15 scans" profile of Fig. 5. Further ageing of the electrode didn't bring about any significant change in Tafel slope – a polarisation curve recorded in 1.0 M NaOH for the electrode characterised by the "After 20 scans" CV of Fig. 5 exhibited a Tafel slope of ca. 45 mV dec^{-1}. The significance, with regard to OER polarisation behaviour, of this variation in voltammetric profile with electrode ageing will be discussed later.

3.4. Steady state polarization measurements : Fe electrode' type' C

It was found that "type" C Fe electrodes characterised by voltammograms similar in profile to the later scans of Fig. 5, facilitated the measurement of reasonably reproducible oxygen evolution steady state polarisation characteristics over a range of NaOH concentrations from 1.0 – 5.0 M – see Fig. 6. For each of these electrolyte concentrations, lower straight line Tafel regions were observed with slopes in the range of 44 – 47 mV dec^{-1} ($\cong 2.303(4RT/5F)$ at 25ºC), in contrast to the situation that prevailed for "type" A electrodes (Fig. 2).

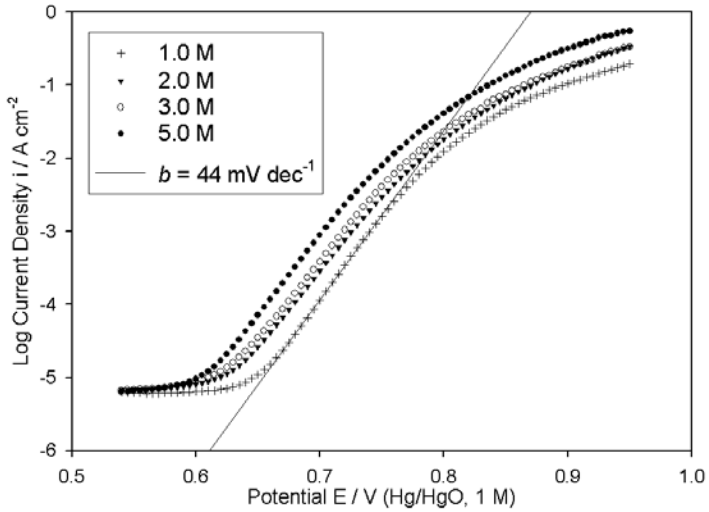

Figure 6. *iR* corrected, OER steady state polarisation curves recorded in the direction of increasing potential for a "type" C iron electrode in NaOH solutions of various concentration.

Reaction order plot were constructed, based upon the data of Fig. 6 at potentials associated with the aforementioned Tafel region. Typical of these plots is that presented in Fig. 7. The linearity of this reaction order plot is not altogether satisfactory, possibly owing to the fact that the Tafel slopes for the 2.0 and 3.0 M NaOH solutions are slightly larger (~ 47 mV dec^{-1}) than those of the 1.0 and 5.0 M solutions (~ 44 mV dec^{-1}). It is however resonable to conclude that the reaction order parameter is approximately unity, and certainly does not approach the non-integral value of $m_{OH^-} \approx 3/2$ noted at lower overpotentials for both multi-cycled and extremely "aged" Fe anodes [4].

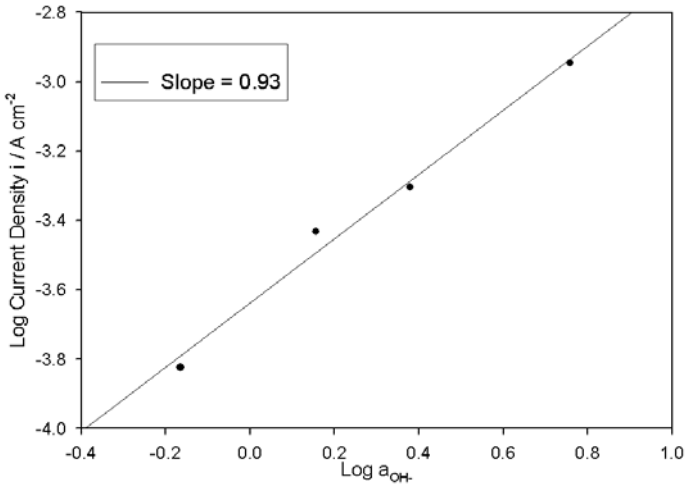

Figure 7. Reaction order plot based on the steady state polarisation data of Fig. 6 at a potential of E = 0.705 V.

3.5. Electrochemical Impedance Spectroscopy (EIS) measurements

Electrochemical impedance spectra, recorded successively in the direction of increasing potential for a "type" A Fe electrode in 1.0 M NaOH solution are presented in the Bode format in Fig. 8. The same data is also plotted in the complex plane (Nyquist) format in Fig. 9. In addition, the EIS responses of a "type" C Fe electrode in 1.0 M NaOH, at various potentials associated with significant oxygen evolution current density, are depicted in Bode format in Fig. 10.

A detailed discussion of the EIS responses of these passive oxide covered Fe (and also Ni and Co) electrodes in the oxygen evolution potential region and the appropriate choice of equivalent circuit model, has been reserved for elsewhere [33]. In the present article our interest is primarily restricted to ascertaining whether or not the Tafel parameters obtained by the dc steady state polarisation technique are supported by ac measurements. To this end CNLS fitting has been performed, of the raw impedance responses to the appropriate equivalent circuit model of Fig. 11. We have also applied these models to the simulation of the interfacial electrical properties of "aged" passive iron electrodes in the OER potential region [4].

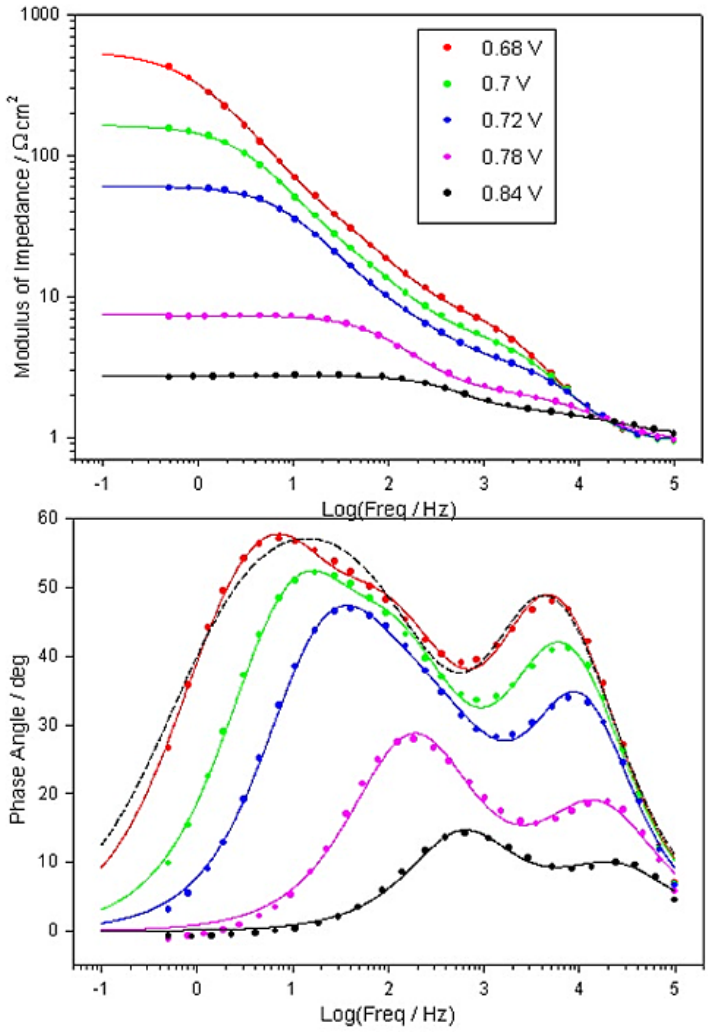

Figure 8. Bode plots recorded at various potentials within the region of significant OER current density for a "type" A Fe electrode in 1.0 M NaOH solution. The raw data is represented by the circles, while the continuous lines plot the optimised transfer functions for the relevant equivalent circuit model (Fig. 11). The dashed line represents the transfer function yielded by attempting to fit the data recorded at 0.68 V to a two RC loop circuit model similar to Circuit B of Fig. 11.

The peak feature at frequencies between 10^3 and 10^5 Hz in the phase angle vs. log frequency Bode plots of Figs. 8 and 10 is indicative of the relaxation of the dielectric properties and resistivity of the passive oxide film. In the Nyquist plots of Fig. 9 this oxide film impedance response is manifested as the smaller, high frequency psuedo-semi-circular feature. The $C_{film}R_{film}$ loop of the equivalent circuits of Fig 11 models these oxide film electrical properties. The various other circuit elements retain the significance assigned to them earlier in this series, when they formed the simpler equivalent circuit models that were sufficient to simulate the impedance response of passive oxide covered Ni [1] and Co [2] OER anodes. Recapping briefly, R_Ω represents the uncompensated electrolyte resistance, while the C_{dl} element models the double layer capacitance. The resistive elements R_p and R_s are related to the kinetics of the interfacial charge transfer reaction [34] and $C_ø$ is the value of a capacitor, which

in parallel with the resistance, R_s, models correctly the relaxation of the charge associated with the adsorbed intermediate(s) [34]. In Figs. 8 – 10, the simulated impedance responses of the equivalent circuit models when the various elements take on their optimised values (for a given potential) are presented as continuous traces, whereas the measured raw data is represented as discrete points.

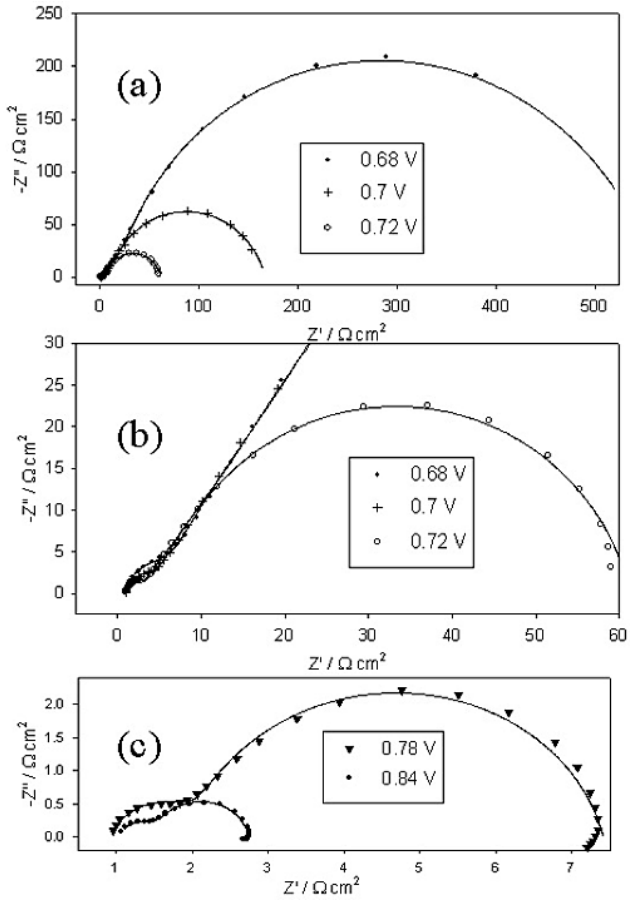

Figure 9. Nyquist representations of the impedance data of Fig. 8; (a) the data recorded at lower overpotentials, (b) a higher resolution view of the aforementioned data, (c) higher overpotential EIS data. Again the continuous lines are generated by the results of the CNLS fitting process, while the discrete points represent the raw data.

In the case of the EIS spectra that we have presented elsewhere [4] for extremely aged Fe OER electrodes, the phase angle vs. log freq. Bode plots were characterised at lower overpotentials by three very distinct capacitance peaks (modelled, in order of decreasing frequency by the C_{film}, C_{dl}, and $C_{ø}$ circuit elements), while equivalently the Nyquist plots comprised of three readily distinguishable pseudo-semi-circular regions. At first glance however, the lower overpotential phase angle vs. log freq. plots of Figs. 8 and 10 seem to possess just two capacitive maxima, while only two semi-circular features are readily evident in the complex plane data of Fig. 9. On this basis it would seem that Circuit A of Fig. 11 contains a superfluous *RC* loop.

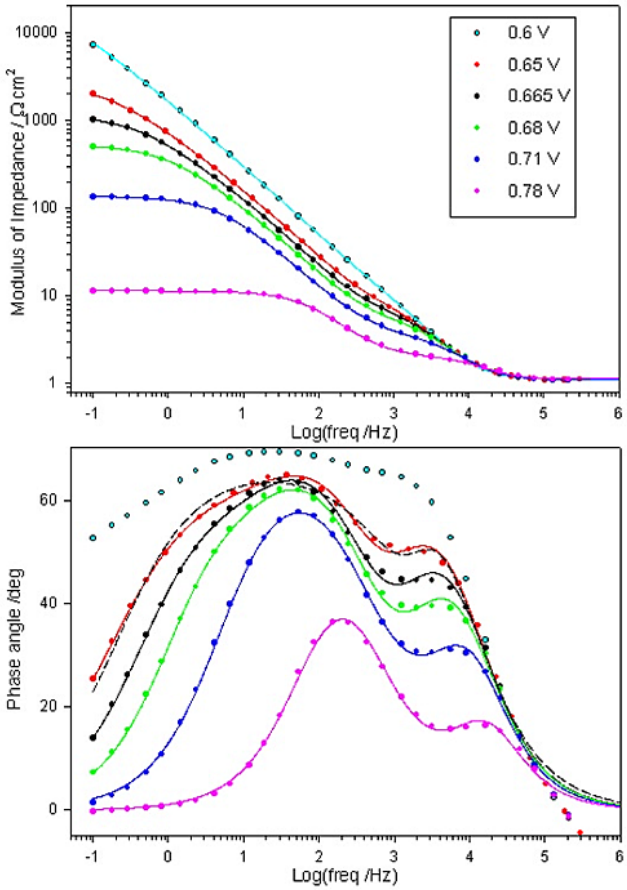

Figure 10. Bode plots recorded at various potentials for a "type" C Fe electrode in 1.0 M NaOH solution. The comments of the caption of Fig. 8 also apply here. The dashed line represents the transfer function obtained by attempting to fit the data recorded at 0.65 V to a two RC loop equivalent circuit model.

In fact the apparent characterisation of two relaxation processes instead of three arises owing to the poor temporal separation of the *RC* time constants related to the relaxation of the charges associated with the double layer capacitance (shorter time constant) and the adsorption pseudo-capacitance (longer time constant). The rather unsymmetrical low frequency peaks (for lower overpotentials) in the phase angle vs. log freq. plots of Figs. 8 and 10, arise not from the impedance response of a single charge relaxation process but from the superposition of the responses of the two aforementioned relaxation processes. In the cases of the spectra recorded at 0.68 V in Fig. 8 and 0.65 V in Fig 10 the results of fitting the data to an equivalent circuit model with just two *RC* loops in series with R_Ω (i.e. similar to Circuit B of Fig 11) are included. Clearly, less satisfactory fitting is obtained for a two serial *RC* loop circuit than for Circuit A. Admittedly, increasing the number of fitting parameters will tend to improve the quality of a CNLS fit, however the aforementioned observation strongly indicates the suitability of Circuit A for the simulation of the properties of electrode/solution interface at lower OER overpotentials.

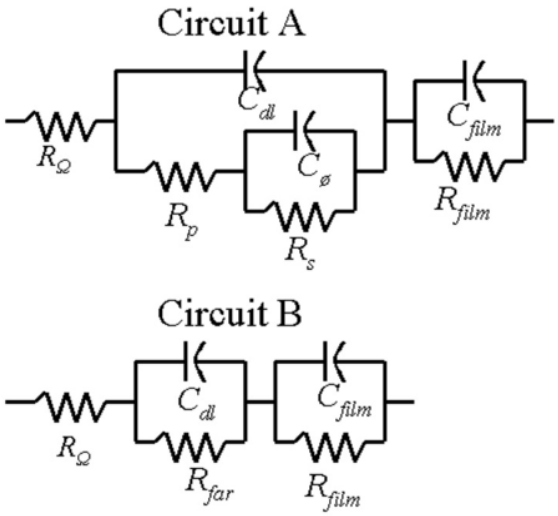

Figure 11. Equivalent circuit models used in the CNLS fitting of the impedance data of Figs. 8 - 10. As discussed in the text, Circuit A reduces to Circuit B at higher overpotentials.

Table 1(a). Optimum fit parameters for the CNLS fitting of the data of figs.8 and 9 to Circuit A (lower overpotentials).

E	R_s	C_ϕ	α	R_p	C_{dl}	α	R_{film}	C_{film}	α	R_Ω
V	Ωcm^2	μFcm^{-2}		Ωcm^2	μFcm^{-2}		Ωcm^2	μFcm^{-2}		Ωcm^2
0.68	446.8	85.2	0.97	110.3	59.3	0.78	4.44	19.65	0.94	0.91
0.7	110.4	135.8	0.98	52.3	85.4	0.81	3.42	18.26	0.92	0.91
0.72	40.6	128.8	0.92	17.5	104.1	0.84	2.25	17.11	0.93	0.94

Table 1(b). Optimum fit parameters for the CNLS fitting of the data of Figs. 8 and 9 to Circuit B (Higher overpotentials).

E	R_{far}	C_{dl}	α	R_{film}	C_{film}	α	R_Ω
V	Ω cm^2	μF cm^{-2}		Ω cm^2	μF cm^{-2}		Ω cm^2
0.78	5.40	245.3	0.86	1.07	20.88	0.85	0.95
0.84	1.20	284.7	0.90	0.49	26.38	0.84	1.05

As in our analysis of the variation in impedance response, with overpotential, for "aged" Fe OER electrodes [4], it is apparent from the phase angle vs. log freq. plots of Figs. 8 and 10 that, as the applied potential is increased, the low frequency psuedo-capacitive contribution diminishes in significance compared to that of the double layer capacitance, and the appropriate equivalent circuit model reduces to Circuit B of Fig. 11, where R_{far} is the total Faradaic resistance. Fitting parameters can

still be obtained for $C_{ø}$ at these higher potentials (E = 0.78 and 0.84 V for the data of Figs. 8 and 10), however the fitting program output indicates that they have little significance. The best-fit values of the equivalent circuit elements for the CNLS fitting of the EIS data of Figs. 8 and 10 are listed in Tables 1 and 2 respectively. A feature common to the equivalent circuit analysis of the present article, and that performed for oxidised Ni [1] and Co [2] OER anodes in the previous parts of this series, is the need to use *constant phase elements* (CPEs) in place of pure capacitors, in order to simulate frequency dispersion in the experimental capacitive response. The depressed nature of the complex plane semicircles of Fig. 9 are indicative of such dispersion, the physical origin of which is believed to lie in electrode surface roughness and inhomogeneities [35]. The mathematical treatment, in terms of the CPE model, of a capacitive process displaying such frequency dispersion takes the form:

$$Z_{CPE} = A(j\omega)^{-\alpha} \tag{8}$$

In eqn. 8, $A = 1/C_{\alpha=1}$, where $C_{\alpha=1}$ is the value of the capacitance in the absence of frequency dispersion, and α is an exponent ($\alpha \leq 1$ for a physically reasonable situation) equal to unity in the case of an ideal capacitor. The result of a CNLS fitting of raw impedance data to a CPE using the SIM program, is an output in the form of optimised values for $C_{\alpha=1}$ and α.

Table 2(a). Optimum fit parameters for the CNLS fitting of the data of CNLS fitting of the data of fig.10 to Circuit A (lower overpotentials).

E	R_s	$C_{ø}$	α	R_p	C_{dl}	α	R_{film}	C_{film}	α	R_{Ω}
V	Ωcm^2	μFcm^{-2}		Ωcm^2	μFcm^{-2}		Ωcm^2	μFcm^{-2}		Ωcm^2
0.65	2719.8	8.2	0.61	208.6	42.5	0.87	4.29	28.13	0.91	1.11
.665	923.0	17.1	0.66	238.3	53.7	0.86	3.83	24.19	0.91	1.11
0.68	338.6	30.0	0.80	182.3	64.1	0.85	3.04	22.31	0.91	1.11
0.71	73.0	48.5	0.81	59.13	86.6	0.85	1.89	20.01	0.94	1.11

Table 2(b). Optimum fit parameters for the CNLS fitting of the data of Fig. 10 to Circuit B (higher overpotentials).

E	R_{far}	C_{dl}	α	R_{film}	C_{film}	α	R_{Ω}
V	$\Omega\ cm^2$	$\mu F\ cm^{-2}$		$\Omega\ cm^2$	$\mu F\ cm^{-2}$		$\Omega\ cm^2$
0.78	9.46	159.7	0.86	0.777	17.88	0.99	1.15
0.84	2.16	165.3	0.85	0.494	14.17	0.98	1.18

In the first part of the series [1], it was shown that, at overpotentials where simple Tafel behaviour prevails, the following expression can be easily derived:

$$\log\left(\frac{1}{R_{far}}\right)=\frac{\eta}{b}+\log\left(2.303\frac{i_0}{b}\right) \quad (9)$$

This equation implies that that the inverse slope of a plot of log ($1/R_{far}$) against η is equal to the Tafel slope b. At lower overpotentials where Circuit A applies, $R_{far} = R_s + R_p$. Therefore the listed fitting parameters of Tables 1 and 2 can be used to verify the values of b obtained by the dc steady state polarisation technique for "type" A and C Fe electrodes respectively. Plots of log ($1/R_{far}$) against η for these two electrodes are presented in Fig. 12. It is apparent that there is excellent agreement between the values of the Tafel slopes obtained from the impedance data, b_{EIS}, and those obtained by the steady state polarisation method, b_{SS}. For the "type" A Fe electrode, b_{EIS} = 41 mV dec^{-1} compared to the value of b_{SS} =39 mV dec^{-1} for the same system (Fig. 2, 1.0 M). In the case of the "type" C Fe electrode in 1.0 M NaOH, b_{EIS} = 45 mV dec^{-1} while b_{SS} = 44 mV dec^{-1} (Fig. 6).

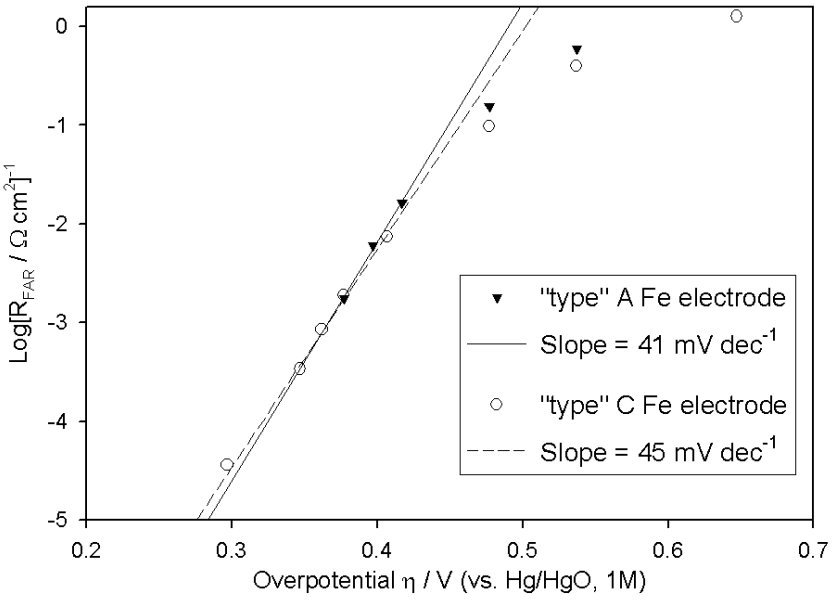

Figure 12. Log $(R_{far})^{-1}$ vs. η plots constructed from the impedance data of Figs. 8 ("type" A electrode) and 10 ("type" C electrode).

3.6. Mechanistic pathway for oxygen evolution

As outlined above, irreproducibility in OER polarisation measurements, rendered more challenging the task of the experimental determination of the kinetic parameters b and m_{OH^-} for relatively un-aged passive oxide covered Fe electrodes, than was the case for passivated Ni [1] and Co [2] electrodes and indeed for multicycled and extremely aged Fe anodes [4]. Summarising briefly, for non-electrochemically pre-treated Fe electrodes ("type" A) the Tafel slope was observed to vary with increasing electrolyte concentration from $2.303(2RT/3F)$ in 1.0 M NaOH to $2.303(4RT/5F)$ in 5.0 M NaOH, thus creating a problem for the meaningful determination of m_{OH^-}. In any case the measured value of i at a given applied potential E was found to vary from experiment to experiment in

the same NaOH solution. At first, the electrochemical pre-reduction of a freshly prepared electrode didn't improve the situation, with b observed to increase progressively from $\sim 2.303(2RT/3F)$ to $\sim 2.303(4RT/5F)$ in 1.0 M NaOH, over the course of the first 10 experiments, despite the application of pre-treatment routine B prior to each experiment. However, it was noted that subsequent to these initial 10 or so experiments, the Tafel slope of $b \sim 2.303(4RT/5F)$ was observed reproducibly in successive measurements and so the electrocatalytic behaviour of the electrode had become stable for the OER ("type" C electrode). Furthermore this same value of $b \cong 2.303(4RT/5F)$ characterised the lower overpotential oxygen evolution polarisation behaviour for various electrolyte solutions where 1.0 M $\leq$ [OH^-] $\leq$ 5.0 M, thus facilitating the determination of a value of $m_{OH^-} = \sim 1$ for the reaction order parameter. Therefore the identification of an OER pathway, the kinetic analysis of which yields $b \sim 2.303(4RT/5F)$ with $m_{OH^-} = 1$, would seem to be a good starting point in the rationalisation of the experimental data for the various iron electrodes.

In fact the aforementioned combination of experimental values of b and m_{OH^-} has already been encountered in the present series for the OER on pre-reduced Co electrodes [2]. As we commented in that case, a Tafel slope of $b \sim 2.303(4RT/5F)$ cannot be reconciled with any of the standard OER mechanisms proposed in the literature, regardless of which step is chosen as rate-determining or whether the Langmuir or Temkin isotherm is admitted to describe the potential dependent coverage of the reaction intermediates – cf. ref. 9, Table II. However, it is possible to account for such a Tafel slope, if a *dual barrier model* of the metallic electrode/solution interface is admitted. One such model that is applicable to the present system proposes that only a fraction of the total potential difference, E, between the metallic electrode and the solution is effective in charge transfer at the electrode/solution interface, with the remainder of the potential drop occurring across an electronically conductive barrier oxide layer, through which the charge passed during the course of the OER must migrate under the influence of an electric field. This model was first developed by Meyer [36] for cathodic processes at oxide covered zirconium electrodes and was subsequently applied by MacDonald and Conway [37] to the OER at gold anodes in both acidic and basic aqueous solutions. We have discussed the model in detail elsewhere [2] and to avoid repetition we provide only a functional outline below.

The model envisages a potential drop of V_f, related to a field driven charge migration process across the barrier oxide, in series with the potential drop, V_s, affecting the electrochemical charge transfer process (i.e. the OER) at the electrode/solution interface. Thus the total applied potential, E, can be expressed as the simple sum: $E = V_f + V_s$. In the normal kinetic analysis (i.e. where the only potential barrier is that to the electrochemical interfacial charge transfer) of a OER pathway, that yields a Tafel slope of $b = 2.303(2RT/3F)$ when a particular step is considered to be rate limiting, the overall current density i at an applied potential E can be written as,

$$i = wi_0 \exp\left[\frac{(1+\beta_s)FE}{RT}\right] \tag{10}$$

where, w is a constant which would be equal to unity, had we chosen to represent the potential in terms of the oxygen overpotential η. If the charge transfer barrier for the rate determining step is considered to be symmetrical, then $\beta_s = ½$, and $b = \partial E/\partial \log i = 2.303(2RT/3F)$.

On the other hand, under the dual barrier model, when the OER is proceeding in the steady state, its RDS must be in equilibrium with the charge transport process across the oxide film. If rate equation (10) is equated with the rate equation for the barrier oxide charge migration process, it can be shown [2, 36] that the overall current density, i, across the two barriers is given by,

$$i = W \exp\left[\frac{(1+\beta_\Sigma)FE}{RT}\right] \tag{11}$$

Where

$$\beta_\Sigma = \frac{\beta_f \beta_s}{\beta_f + \beta_s} \tag{12}$$

and W is a constant, the nature of which we outlined previously [2]. In eqn. 12, β_f is the symmetry factor for the field assisted migration of the charge carriers in the barrier oxide film, and so the β_Σ term has the significance of an *overall symmetry factor* taking account of the two charge transfer barriers. If we adopt the usual assumption that both of these barriers are symmetrical, then $\beta_s = \beta_f = ½$ and so $\beta_\Sigma = ¼$. Inserting this value of β_Σ in eqn. 11, and performing a logarithmic analysis yields a value of $b = \partial E/\partial \log i = 2.303(4RT/5F)$, where dual barrier conditions prevail. It can therefore be concluded, that if the dual barrier model applies to oxygen evolution at our "type" C Fe electrodes, then the observed Tafel slope of $2.303(4RT/5F)$ is indicative of a pathway (with a given RDS) which leads to a prediction of $b = 2.303(2RT/3F)$ when the more usual "single barrier" type of kinetic analysis is applied.

MacDonald and Conway [37] didn't extend their analysis to the effect of the dual barrier model on the predicted value of the reaction order, However after Meyer [36], we have shown [2] that under dual barrier conditions, the experimentally measured reaction order with respect to the activity, a_s, of a particular reactant species in the electrochemical charge transfer reaction, $(\partial \log i/\partial \log a_s)_E$, is given by the expression,

$$\left(\frac{\partial \log i}{\partial \log a_s}\right)_E = \frac{m_s \beta_f}{\beta_f + \beta_s} \tag{13}$$

where, m_s, is the value that would be measured for the relevant reaction order in the absence of the oxide film charge transport related potential barrier. If we again assume that $\beta_f = \beta_s = ½$, then the quantity $\beta_f/\beta_f + \beta_s = ½$. Substituting the measured value of $(\partial \log i/\partial \log a_s)_E \approx 1$ into eqn. 13, therefore yields $m_s = 2$. This leads to the conclusion, that if we admit the dual barrier model to explain the explain the "anomolous" experimental Tafel slope of $b = \sim 2.303 \times 4RT/5F$, then this measured value of b and its associated OH^- reaction order of unity, point to the applicability of an OER pathway, the

conventional (single barrier) kinetic analysis of which, yields predictions of b = 2.303×2RT/3F and m_{OH^-} = 2.

As we discussed when dealing with the experimental data obtained for pre-reduced Co electrodes [2], several of the commonly proposed OER pathways can account for the aforementioned kinetic parameters, where in each case a particular step is considered to be rate determining with a low fractional coverage (i.e. $\theta \rightarrow 0$) of the reaction intermediates prevailing – c.f. Table II of ref. 9. For these Co anodes, a clue to the most likely pathway was provided by experimental data obtained for the OER on aged electrode specimens – at lower overpotentials it was found that b = ~60 mV dec^{-1} (≈ 2.303×RT/F at 25°C) with m_{OH^-} = ~3/2, while for higher potentials the observed values of these parameters were b = ~120 mV dec^{-1} (≈ 2.303×2RT/F at 25°C) with m_{OH^-} = ~1. Recall from the introduction to the present article, that we have observed an identical set of OER kinetic parameters for multi-cycled and "aged" Fe electrodes[4] and have rationalised it in terms of the physisorbed hydrogen peroxide pathway (A). Thus it would appear that *passive oxide covered Co and Fe electrodes exhibit very similar OER polarisation behaviour*, with relatively un-aged, pre-reduced anodes characterised by b = ~2.303×4RT/5F and m_{OH^-} = ~1 (equivalent to b = ~2.303×2RT/3F and m_{OH^-} = ~2 when the dual barrier effect is factored out) at lower overpotentials, which alters with ageing to b = ~2.303×RT/F and m_{OH^-} = ~3/2 in this same lower overpotential range, while for the "aged" electrodes at higher overpotentials, a second straight-line Tafel region (b = ~2.303×2RT/F and m_{OH^-} = ~1) is also reproducibly resolved. In our communication on the OER at Co electrodes [2], it was shown that a mechanism very similar to pathway (A) could account for the experimental data observed for the relatively fresh Co electrodes as well as for the aged anodes of the same metal. A pathway analogous to that proposed for Co [2], is outlined below for oxide covered Fe electrodes:

$$\left[Fe(VI)O_m(OH)_n\right]^{p-} + OH^- \rightarrow \left[Fe(VI)O_m(OH)_{n+1}\right]^{p-} + e^- \quad \text{(BI)}$$

$$\left[Fe(VI)O_m(OH)_{n+1}\right]^{p-} + OH^- \rightarrow \left[Fe(VI)O_m(OH)_n - H_2O_2\right]^{p-} + e^- \quad \text{(BII)}$$

$$\left[Fe(VI)O_m(OH)_n - H_2O_2\right]^{p-} + OH^- \rightarrow \left[Fe(VI)O_m(OH)_n - HO_2\right]^{p-} + H_2O + e^- \quad \text{(BIII)}$$

$$\left[Fe(VI)O_m(OH)_n - HO_2\right]^{p-} + OH^- \rightarrow \left[Fe(VI)O_m(OH)_n\right]^{p-} + O_2(g) + H_2O + e^- \quad \text{(BIV)}$$

The important features of this mechanism are as follows:

- Following the practice of the previous instalments of this series, the catalytically active and intermediate species are represented as complex anionic entities, where, in the present case; p=2m+n-6. We believe that this approach is more realistic than thinking in terms of discrete simple stoichiometric oxy-hydroxide species. In the review of the electrochemistry of iron electrodes earlier in this article, the super-nernstian shift displayed by the A3/C2 voltammetric peak pair was discussed. This phenomenon is indicative of the coordination of extra hydroxide ions from solution, by the surface species of the passive oxide formed at anodic potentials on Fe electrodes at high pH. Our proposal that the reactive sites for oxygen evolution at oxidised Fe electrodes are centred on Fe(VI) species, has also appeared earlier in this article and was discussed in detail elsewhere [4]. As with pathway (A),

$-H_2O_2$ represents *physisorbed* hydrogen peroxide.

- For cobalt, we demonstrated [2] that such a mechanism (identical to (B), except developing from a $[Co(IV)O_m(OH)_n]^{p-}$ (p=2m+n-4) active site in step I) can account for $b = 2.303(2RT/3F)$, and $m_{OH^-} = 2$, where the second step is considered to be the RDS, with $\theta \rightarrow 0$.
- As outlined in the Introduction and discussed in detail elsewhere [4], the kinetic parameters for "aged" Fe (and also aged Co [2]) anodes can also be rationalised by admitting the physisorbed hydrogen peroxide type of mechanism with the second step rate limiting. A formal kinetic analysis [4] shows that $b = 2.303(RT/F), m_{OH^-} = 3/2$ is expected if an intermediate fractional coverage of reaction intermediates is achieved ($0.2 \leq \theta \leq 0.8$), changing to $b = 2.303(2RT/F), m_{OH^-} = 1$ where full surface coverage is approached ($\theta \rightarrow 1$).
- As previously mentioned, mechanism (B) is only one of several candidate pathways which can account for the measured kinetics in the case of the relatively un-aged Fe electrodes dealt with in this article. However, the physisorbed peroxide mechanism ((A) or (B)) is, to the best of our knowledge, uniquely capable of accounting for the experimental value of b = ~60 mV dec^{-1} with m_{OH-} = ~3/2, observed for aged Fe [4] and Co [2] electrodes. In view of this, we have previously proposed [2] for oxidised Co electrodes, that a pathway analogous to (B) is most likely to be that operative for the OER. This prediction was made on the basis that regardless of electrode age, or passive oxide film thickness, one is fundamentally dealing with electrocatalysis at the surface of a rather hydrated cobalt oxyhydroxide film and therefore the nature of the active sites and the reaction mechanism should remain unchanged. Changes in b and m_{OH-} with electrode ageing at lower oxygen overpotentials, therefore occur, not due to a change in reaction mechanism, but instead due to a change in the appropriate intermediate adsorption isotherm from Langmuir ($\theta \rightarrow 0$) for fresher electrodes to Temkin ($0.2 \leq \theta \leq 0.8$) for aged anodes. This logic should also apply to the Fe electrodes considered in the present article, and to the "aged" and multi-cycled Fe anodes described elsewhere [4]. *We therefore propose that pathway B* (with step (B II) as the RDS) *is the most likely mechanism for oxygen evolution at oxidised iron electrodes* in aqueous alkaline solution.
- As we also discussed for Co electrodes [2], the aforementioned change, with ageing, in the applicable lower overpotential adsorption isotherm for Fe anodes from Langmuir to Temkin, is most likely related to the development of an increasingly hydrated and dispersed outer oxide phase with repeated polarisation – recall the earlier review on Fe electrochemistry and the "residual oxide" concept discussed therein. Indeed we have interpreted the differences in the voltammetric profiles obtained for fresh and "aged" Fe electrodes in alkaline solution, on this basis [4]. Furthermore, there is no doubt that the oxide film produced by the potential multi-cycling of an Fe electrode will be significantly more hydrated [4, 8] than that obtained by the passivation of relatively un-aged Fe surfaces as outlined for the anodes of the present article in the Experimental section. The amount of

amphoteric character displayed by an anodic oxide is expected to be proportional to its degree of hydration [4, 8, 24]. It is therefore expected that "aged" and multi-cycled Fe electrodes would contain a larger surface density of the catalytically active, complex anionic $[Fe(VI)O_m(OH)_n]^{p-}$ species at lower overpotentials, relative to fresher Fe electrodes.

- Pathway (B) has been devised in preference to the original physisorbed hydrogen peroxide mechanism, (A), because in the case of the latter, it is intuitively rather difficult to understand how the chemical recombination step, (A IV), could proceed at a sufficient velocity under low coverage Langmuir conditions, such as not to render it rate-limiting for the entire process. We have commented further on this matter previously [2]. It is worth noting that when Bockris and Otagawa [9] originally outlined scheme (A), their kinetic data was suggestive of the applicability of the Temkin adsorption isotherm at lower overpotentials and thus the aforementioned reservation didn't arise.

3.7. The physical origin of the oxide charge transport barrier

When discussing the differences in the OER steady state polarisation behaviour of "type" B and C Fe electrodes in 1.0 M NaOH (Fig. 4), we commented without further elaboration, that a comparison of the "After 4 scans" ("type" B) voltammetric trace of Fig. 5 with the later profiles of the same figure (now characteristic of a "type" C anode) could be useful in elucidating this matter. Of particular interest is the fact that the A3/C2 peak pair is significantly more prominent (i.e. is characterised by a greater associated redox charge capacity Q) in the voltammogram for the "type" B electrode, relative to the profiles for the more aged anodes ("type" C). We recall from the review of the electrochemistry of Fe electrodes presented earlier in this article, that this peak pair has been attributed to the formation and reduction of an outer, dispersed, hydrous Fe(III) based oxy-hydroxide layer [4, 8].

By contrast, the A4 anodic feature has a significantly larger associated charge in the "type C" voltammetric profiles compared to the trace for the fresher electrode. Recall that the A4 anodic "shoulder" has been attributed to the oxidation of the initially formed Fe(II) based passive oxide, to anhydrous phases of Fe(III) based oxide or oxy-hydroxide species, located in the inner region of the film. It can therefore be concluded that that the inner compact oxide region has a larger relative influence on the surface electrochemistry of the "type" C iron electrode (with its associated OER Tafel slope of $\square\ 2.303(4RT/5F)$), than the "type" B anode (associated Tafel slope of $\square\ 2.303(2RT/3F)$). On this basis, it seems reasonable to connect the rise in Tafel slope with electrode ageing, to a simultaneous increase in the influence of the compact anhydrous oxide on the overall properties of the metallic electrode/oxide film/electrolyte solution complex interface. In other words, we are making an identification of the oxide film charge migration barrier with the inner compact anhydrous region of the anodic oxide film, or with the interface between this inner region, and the outer more disperse and hydrated region of the film. In fact, on the basis of voltammetric data, we have previously reached an identical conclusion in the case of the OER at passive oxide covered Co electrodes [2]. In that article

we commented that, under the dual layer structural model for anodic oxides proposed by Burke et al.[25 – 27], the inner region is envisaged to consist of a rigid network of polar covalent bonds, through which ionic transport is difficult – such a model is consistent with the "barrier oxide" of the analyses of Meyer [36] and MacDonald and Conway [37]. On the other hand, the outer dispersed region of the oxide is considered to have a structure similar to that of redox polymers, with electron transfer along the "polymer" strands facilitated by self exchange between neighbouring oxy metal groups – we have demonstrated elsewhere [4] that the average diffusion coefficient for charge percolation through anodically generated hydrous iron oxy-hydroxide films is similar in magnitude to that reported for electronically conductive organic polymers such as polyaniline or poly(pyrrole).

While the increase in OER Tafel slope, which accompanies the ageing of "type" B to "type" C Fe electrodes, can be rationalized in terms of the simultaneous increase in the influence of the anhydrous inner region on charge transport across the oxide film, it is clear that such an explanation is inadequate with regard to the variation of Tafel slope with OH^- concentration observed for fresh "type" A anodes in Fig. 2. The latter effect is more difficult to explain, since, for these electrodes there were no pre-treatment CVs – recall that prior to steady state polarisation experiments, "type" A anodes were subject to mechanical polishing only. Instead, in an attempt to understand the aforementioned experimental observations, we appeal to our experiences [4] with hydrous oxide films generated by the repetitive potential cycling of an iron electrode in NaOH solutions of various concentrations.

For such oxide films, voltammetry experiments were conducted to examine the influence of OH^- ion concentration on the extent of hydrous film growth, which was quantified in terms of the charge capacity, Q, evaluated by integration of the A3 anodic peak. In the case of oxide layers grown for a shorter activation time (5 minutes) a maximum charge capacity was observed at $[OH^-] = 1.0$ M. However for layers grown for 20 minutes the maximum value of Q was noted for $[OH^-] = 0.1$ M, with a sharp decrease in charge capacity with increasing hydroxide ion concentration. On the basis of these results we postulated that the behaviour noted for longer times was due to a suppression of hydroxide dissociation with increased OH^- ion concentration, causing an inhibition of crystallisation of the hydrous outer layer. This in turn leads to the formation of a more amorphous film structure that is more effective in excluding water from the inner region of the film, thereby inhibiting the growth of the dispersed outer hydrous layer. The net effect of this is that the inner compact layer will have an increasing influence on the overall surface electrochemistry of an Fe electrode with increasing OH^- concentration. Thus the explanation for the increase in Tafel slope for "type" A Fe electrodes with increasing NaOH solution concentration, may be effectively equivalent to that forwarded for the similar Tafel slope increase that accompanies electrode ageing. It is recognised however, that drawing direct parallels between the growth of oxide films by repetitive potential cycling, and their growth during slow potential stepping experiments associated with recording of steady state polarisation curves, may not be an entirely valid exercise.

The oxide film resistance R_{film}, as characterised by EIS should *not* be identified with the resistance of the barrier layer as discussed above. This is demonstrated by the Tafel plot for the "type" C electrode in Fig. 12. The dual barrier Tafel slope value of $b = \sim 2.303 \times 4RT/5F$ is obtained in this case even though the analysis is based only on R_{far} (see eqn. 9) which does not include R_{film}. In fact the fitted values of R_{film} are so small compared to R_{far} ($=R_p + R_s$ at lower η) that plotting $\mathrm{Log}[(R_{far} + R_{film})^{-1}]$

vs. η rather than Log[R_{far}^{-1}] vs. η makes practically no difference to the Tafel slopes presented in Fig. 12. Furthermore, no high frequency $R_{film}C_{film}$ impedance response is observed for oxidised Co anodes [2] even though the dual barrier model also applies to this system. The physical origin of the $R_{film}C_{film}$ relaxtion process for passive oxide covered Fe electrodes is discussed elsewhere [33].

3.8. Estimation of electrode roughness factors

At the beginning [1]of the present series of articles, one of the stated aims was the performance of a comparative analysis of the oxygen evolution performance of passive oxide covered Ni, Co and Fe electrodes. Clearly if this is to be conducted in a meaningful manner it is necessary to normalize the recorded values of the OER current (as a function of overpotential) to the active electrode surface area as opposed to the geometric surface area. However as was discussed in an IUPAC commission report [38], the experimental evaluation of electrode roughness factors, f_r, is a rather imprecise science and this is particularly true for electrodes of base metals covered by anodic oxide films, for which there is a scarity of applicable techniques. In view of this, we have turned to a rather novel in-situ approach (the OH_{ads} desorption method) originally proposed by Ho and Piron for the estimation of the active surface areas for the OER, of electrodeposited Ni, Co and Ni-Co alloy electrodes [12]. As we previously discussed for our Co electrodes [2] and some of our Ni anodes [1], the significant deviation from unity of the values of the double layer CPE α parameter listed in Tables 1 and 2, indicate that application of the double layer capacitance ratio method is probably not viable for a meaningful estimation of f_r for our oxidised Fe electrodes.

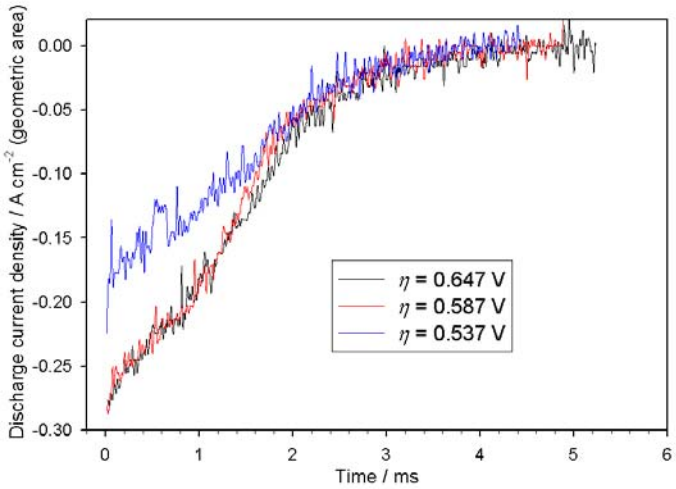

Figure 13. Raw decay current transients for a "type" B Fe electrode in 1.0 M NaOH solution. Indicated are the overpotentials corresponding to the values of i_{appl} in each case.

A detailed discussion of the OH_{ads} desorption technique and the assumptions upon which it is based, has been provided in our article on the OER at passive oxide covered Ni anodes [1] – here we restrict ourselves to a brief outline. The experimental approach involves the galvanostatic charging of

the working electrode at a number of current densities, i_{appl}, corresponding to the OER proceeding in the steady state at known overpotentials η. Upon interruption of the charging current, the electrode is allowed to discharge to ground through a 1Ω series resistor, with the cathodic decay current–time (*i*-*t*) transient recorded by a digital storage oscilloscope connected across the resistor. Integration of this transient between the time of termination of the polarisation and that at which the decay current becomes zero, yields a value for the total charge, Q_{dec}, passed during the course of the discharge process, which is envisaged to occur by the desorption of the intermediate species involved in the OER.

Referring to the voltammograms of Figs. 1 or 5, recorded for Fe electrodes in 1.0 M NaOH solution, it is obvious that the peaks associated with the Fe(II)↔Fe(III) transition (i.e. A3, A4, C1 and C2) occur at potentials significantly cathodic to the oxygen electrode reversible potential of 0.303 V (vs. Hg/HgO, 1 M OH^-). Indeed we have previously shown [8] that in 1.0 M NaOH solution, the peak potential for the A3 anodic feature increases steadily from ~ -0.6 to ~ -0.4 V over a range of voltammetric scan rates from 1 mV s^{-1} to 400 mV s^{-1}. The foregoing observations indicate strongly that desorption of the OER intermediate species from an iron electrode in 1.0 M NaOH solution (upon the interruption of a galvanostatic polarising current density associated with the OER proceeding at a significant rate in the steady state), will involve the discharge of the active oxide surface Fe sites to the +3 oxidation state, from a higher valance state. Recall from mechanism (B), that we have postulated that this higher state is the Fe(VI) state which is stabilised at the oxide surface (at high anodic potentials in concentrated alkaline solution) by existing in the form of an anionic hydroxylated surface complex represented as $[Fe(VI)O_m(OH)_n]^{p-}$. A suitable overall discharge reaction, consistent with mechanism (B), can thus be written as,

$$\left[Fe(VI)O_m(OH)_{n+1}\right]^{p-} + H_2O + 4e^- \rightarrow \left[Fe(III)O_{m-1}(OH)_{n-1}\right]^{p-} + 4OH^- \qquad (14)$$

where, it is considered that desorption of the $[Fe(VI)O_m(OH)_{n+1}]^{p-}$ intermediate (the only one likely to achieve a significant fractional coverage of the active surface since it is consumed in the RDS), facilitates the discharge process.

From Fig. 14, it is obvious that plots of Q_{dec} vs. η are characterised by a steady increase in Q_{dec} with increasing η for lower values of the latter. In such discharge experiments for Ni [1] and Co [2] OER anodes, a plateau was observed in the Q_{dec} vs. η plots in the higher overpotential region characterised by the onset of limiting current behaviour in the associated log$i(\eta)$ characteristic for the same system. The technique of Ho and Piron [12] is based on their proposal that the plateau in such Q_{dec} vs. η plots, corresponds to the desorption of the electrosorbed intermediate (OH_{ads}) for the situation where the coverage of this species approaches a full monolayer. They further proposed that for a two electron desorption process, a resonable *estimate* of the roughness factor is given by the expression, $f_r = Q_{dec}$(plateau)/420μC cm^{-2}, where Q_{dec}(plateau) is the average charge density associated with the plateau region of the Q_{dec} vs. η plot and 420 μC cm^{-2} is a "benchmark" theoretical value, due originally to Fedorova and Frumkin [39], for the charge passed during the two electron deposition or desorption of a monolayer of OH_{ads}. We have previously applied the above formula to estimate roughness factors for passive oxide covered Ni [1] and Co [2] electrodes.

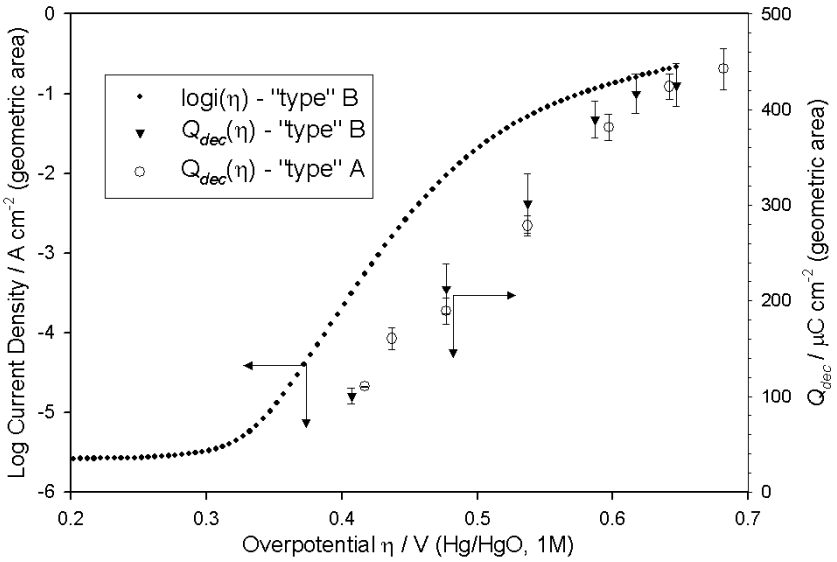

Figure 14. Plots of the total charge, Q_{dec}, passed during the discharge of "types" A and B Fe electrodes in 1.0 M NaOH vs. oxygen evolution overpotential η. Also included is the steady state polarisation curve for the "type" B electrode.

Raw discharge current decay transients are presented in Fig. 13, recorded for a "type" B Fe electrode in 1.0 M NaOH following the interruption of prior anodic charging current densities, corresponding to the overpotentials indicated in the legend. The overall results of this experiment are graphed as a Q_{dec} vs. η plot in Fig. 14, along with the closely related steady state polarisation curve (log$i$ vs. η) for the same system – the latter curve was previously presented in Fig. 4. Also included is $Q_{dec}(\eta)$ data for a "type" A Fe anode in 1.0 M NaOH solution. The $Q_{dec}(\eta)$ data points represent the mean value of Q_{dec} calculated from four transients, recorded in separate experiments, for each value of i_{appl}, while the vertical error bars span ± one standard deviation from this mean. The Q_{dec} vs. η plots of Fig. 14 are not characterized by very obvious plateau regions at higher η, as was the case for Ni [1] and Co [2] anodes at comparable overpotentials. Nonetheless it is apparent for the "type" B data of Fig. 14, that the rate of change of Q_{dec}, with increasing η, becomes small in the higher overpotential range where a limiting current density is approached in the steady state polarisation curve – the same was observed to be true for the data recorded for the "type" A electrode, although in the interests of clarity of presentation the log$i$ vs. η plot has been omitted in this case. It would therefore seem to be resonable for both "type" A and B electrodes, to use the value of Q_{dec} measured at the highest investigated overpotential for the estimation of f_r. Since, according to eqn. 14, we envisage the discharge of Fe OER anodes to occur by the passage of 4 moles of electrons per mole of active sites, instead of 2 moles of electrons per mole of electrocatalytic centres as was the case for Ni [1] and Co [2] electrodes, it is necessary to double the "benchmark" value of 420 μC cm^{-2} with the result that the expression for the estimation of the roughness factor becomes,

$$f_r = \frac{Q_{dec}(plateau)}{840\ \mu C\, cm^{-2}} \tag{15}$$

in the case of iron.

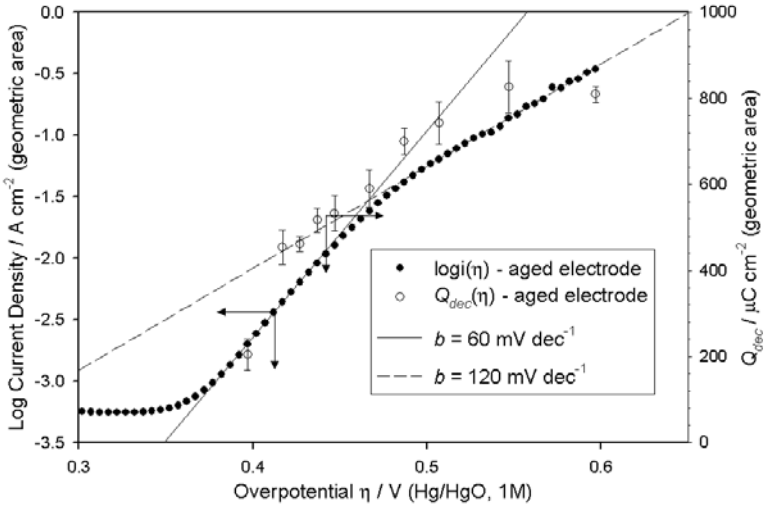

Figure 15. The total charge, Q_{dec}, passed during the discharge of an "aged" Fe electrode in 1.0 M NaOH vs. oxygen evolution overpotential η. Also included is the steady state polarisation curve for this system.

Roughness factor estimation experiments were also conducted for an extremely aged iron electrode – the "type" which (as described above but dealt with in detail elsewhere [4]), is characterised in OER steady state polarisation experiments by a Tafel slope of ~60 mV dec^{-1} at lower overpotentials and a second straight-line region with b = ~120 mV dec^{-1} at higher potentials. A plot of Q_{dec} vs. η, based on transient decay experiments conducted for such an electrode in 1.0 M NaOH is presented in Fig. 15, along with the steady state polarisation curve for the same system. Taking for Q_{dec}(plateau), as discussed above, the values of Q_{dec} associated with the highest investigated overpotential, roughness factors were calculated for the "type" A and B electrodes and also for the aged Fe anode. The results are tabulated in Table 3. As we pointed out in the previous articles [1, 2] of this series, the quoted error refers simply to the experimental error – the true error is likely to be significantly greater, owing to the questionable nature of some of the assumptions on which the OH_{ads} desorption method is based [12].

Table 3. Summary of the roughness factors, f_r, determined for "aged" and "type" A and B iron electrodes in 1.0 M NaOH solution, using the OH_{ads} desorption method.

Fe Electrode "type"	Q_{dec}(plateau) μC cm^{-2}	f_r
A	440 ± 20	0.52 ± 0.02
B	430 ± 20	0.51 ± 0.02
AGED	820 ± 70	0.98 ± 0.08

The estimation of sub-unity roughness factors for the "type" A and "type" B electrodes implies that only a fraction of the geometric surface area (and thus an even smaller fraction of the real oxide surface area, since this is likely to be, at least, somewhat greater than the geometric area) is catalytically active towards the OER for these anodic oxide covered Fe electrodes in 1.0 M NaOH. This conclusion is not altogether surprising, given the model that we proposed above for the catalytically active sites on the surface of the passive iron oxyhydroxide film. Recall that we have envisaged that the somewhat acidic nature of the iron oxide film in solutions of high pH, allows for the stabilisation of Fe(VI) metal centres as part of anionic surface complex species (represented as $[Fe(VI)O_m(OH)_n]^{p-}$) at high anodic potentials. However since it is known [40-42] that soluble Fe(VI) ions (probably in the form of FeO_4^{2-}) are formed at Fe electrode surfaces in aqueous alkaline solution at high anodic potentials, it is likely that only a fraction of the surface Fe(VI) species will be stabilised by coordinating extra OH^- ions, and thus only this fraction of surface sites are available for the catalysis of oxygen evolution, leading to the observed fractional values of f_r.

Compare this to the situation that prevails at the oxide surface on Co electrodes, for which we have proposed [2] the same type of OER pathway as that operative at the passive oxide surface on Fe. For Co, there is a general acceptance that the anodic voltammetric peak at potentials from ca. 0.4 V (vs. Hg/HgO) upwards from which the rising edge of the OER current develops at yet higher potentials, is due to the formation of Co^{4+} ions in the surface region of the oxide film. We have previously [2] represented these species as hydroxylated anionic surface complexes, $[Co(IV)O_m(OH)_n]^{p-}$, the central Co^{4+} ion of which, we envisaged to be the active centre for oxygen evolution. The fact that the formation of these species gives rise to a voltammetric peak at potentials below the rising edge of the oxygen evolution current, indicates that it is appropriate to think in terms of a relatively stable surface phase of Co(IV) species, that can achieve a significant fractional coverage of the electrode *real* surface area. This was in turn, found to lead to roughness factors well in excess of unity, for the catalytically active area relative to the geometric area [2]. On the other-hand an anodic voltammetric peak is generally not observed for the formation of the $[Fe(VI)O_m(OH)_n]^{p-}$ species (although see ref. 4), implying that these species are rather unstable surface entities and that it is inappropriate to think in terms of the existence of a complete surface layer of an Fe(VI) based oxide.

Our contention, that only a fraction of the surface areas of "type" A and B Fe electrodes are active, with respect to the electrosorption of the OER intermediate species, is somewhat reminiscent of the situation known to prevail for the hydrogen evolution reaction at Pt [43, 44] and Ni [45] electrode surfaces. For these systems, it was deduced that the adsorption of overpotential deposited H atoms occurred only on some active fraction of the total number of metallic surface atoms. It should be noted however, that this does not render inapplicable the postulation of high coverages of intermediate species ($\theta \rightarrow 1$) in kinetic mechanistic analyses, i.e. limitingly low or high (Langmuir isotherm) or indeed intermediate (Temkin isotherm) fractional coverages with respect to the total available number of *active* sites, can still be envisaged [45].

Recall that in explaining the different values of b and m_{OH^-}observed for the extremely aged Fe electrode relative to the less aged electrodes (types A, B and C), it was speculated (the fifth bullet point in the discussion of mechanism (B)) that the oxide surface of the former was rougher and more hydrated than that of the other Fe electrodes, and that this facilitated the existence of a relatively larger

concentration of the $[Fe(VI)O_m(OH)_n]^{p-}$ species. In turn this was forwarded as the reason for the applicability of the Temkin adsorption isotherm to the aged electrode, over a range of overpotentials, at which electrosorption at the fresher electrodes was envisaged to follow the low coverage Langmuir isotherm. If this scenario is accurate, then the aged Fe electrode would be expected to have a larger associated roughness factor, as estimated by the OH_{ads} desorption method, and by referring to Table 3, it is obvious, that this is indeed the case.

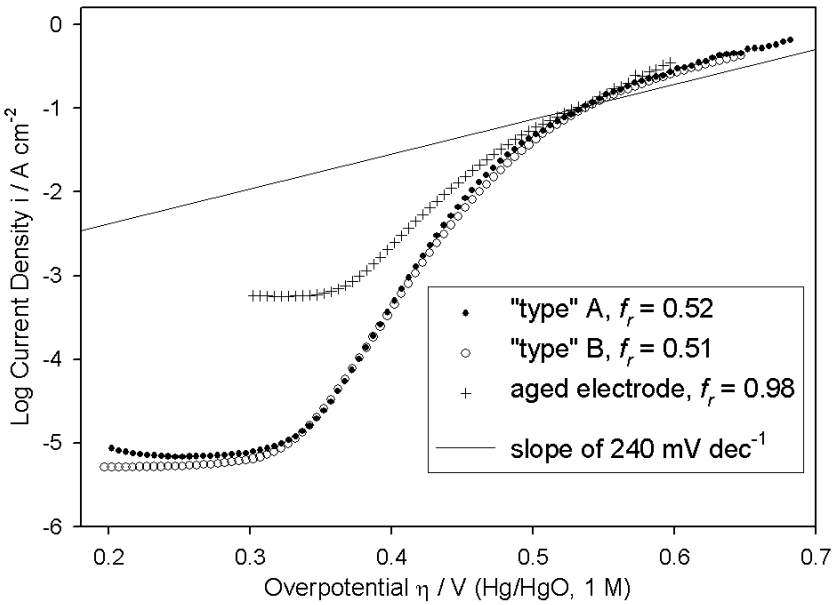

Figure 16. *iR* corrected steady state polarisation curves recorded in 1.0 M NaOH solution, for "aged" and "types" A and B iron electrodes. The values of log $i(\eta)$ are normalised to the estimated truly active surface areas, based on the stated roughness factors.

It is also interesting in this regard to compare the active surface area normalised steady state polarisation characteristics for the different "types" of Fe anodes – see Fig. 16. At an overpotential of η = 0.382 V, both of the fresher electrodes ("types" A and B) exhibit an OER current density of i = 0.138 mA cm^{-2} and a Tafel slope of $\square\ 2.303(2RT/3F)$, which as discussed above, is characteristic of a rate limiting step (B II) with $\theta \rightarrow 0$. At the same overpotential for the aged electrode, $b \cong 2.303(RT/F)$, which we have proposed to arise due to the same RDS proceeding under Temkin adsorption conditions ($0.2 \leq \theta \leq 0.8$). If this is true the current density should be significantly greater for the aged, relative to the fresh electrodes at this overpotential – this clearly is the case with a recorded value for the former of i = 1.158 mA cm^{-2}. This is again consistent with our hypothesis of the previous paragraph, that *at this lower overpotential*, Temkin adsorption is possible for the aged electrode due to a greater surface density of stabilised $[Fe(VI)O_m(OH)_n]^{p-}$ sites in comparison to the fresher anodes, for which adsorption is restricted to the low coverage Langmuir model. However as the overpotential is increased, the complex, hydroxylated Fe(VI) surface sites are induced (i.e. effectively "switched on" for the chemisorption process of step (B I)) at a greater rate for the fresher electrodes, with the result that similar, active surface area adjusted, OER performances are observed for all the anodes at $\eta \geq$ ~0.5 V.

The latter region of potential is associated with the b = ~120 mVdec^{-1} Tafel slope in the case of the aged electrode – as demonstrated elsewhere [4] this value of b arises where a rate determining step, identical or similar to (B II), proceeds in the limit of a fractional coverage θ of unity – i.e. where all (or almost all) surface sites are occupied, that have the potential to adsorb an OH entity according to step (B I). For the polarisation curves of the "type" A and B electrodes, while there is close convergence with the aged anode curve for $0.52 \leq \eta \leq 0.58$ V, such a ~120 mVdec^{-1} upper Tafel region is not apparent. This may however be explained by the observation of a straight line region with $b \cong 2.303(4RT/F)$ (= ~236 mVdec^{-1} at 25ºC) in the case of these relatively unaged anodes. We have previously shown for Co OER electrodes [2] that such a Tafel slope arises, where, again, an RDS equivalent to step (B II) with $\theta \rightarrow 1$ is admitted, but in this case under dual barrier conditions. Thus, for the "type" A and B polarisation curves of Fig. 16, it would seem that while the oxide film charge migration barrier does not apply at lower overpotentials (as evidenced by Tafel slopes of $\cong 2.303(2RT/3F)$, it does prevail at higher η as indicated by the observation of $b \cong 2.303(4RT/F)$ rather than $b \cong 2.303(2RT/F)$ for $\theta \rightarrow 1$. This transition may occur due to dehydration of the oxide film accompanying the gassing reaction, resulting in an increasingly anhydrous, "barrier", type oxide film, as the potential is raised. By contrast, for the aged electrode, the disturbed and inhomogenious nature of the surface (recall the "residual oxide" concept) does not facilitate the formation of a well organised, anhydrous, rigid, polar covalent based oxide phase, and so even at higher overpotentials the dual barrier concept is inapplicable.

3.9. The activity series of the anodic oxides of Ni, Co and Fe for the OER in alkaline solution

Oxygen evolution steady state polarisation curves, with the current density normalised to the active surface area through the indicated roughness factors, are plotted on the same graphs for fresh non-electrochemically pre-treated (Fig. 17) and pre-reduced (Fig. 18) Ni, Co and Fe electrodes in 1.0 M NaOH at 25°C. The data for Ni and Co were originally presented in refs. 1 and 2 respectively. For the purpose of comparison, the same polarisation curves, where the values of log$i(\eta)$ are referred to the geometric surface area are also depicted in the aforementioned figures. Some parameters, relevant to the comparison of the OER catalytic efficiencies of the various electrodes are listed in Tables 4 and 5, for the non-pre-treated and pre-reduced electrodes respectively.

The electrocatalytic activities of different electrode materials for a given reaction are normally compared in terms of the experimentally observed values of the exchange current density i_0. However, as was pointed out by Conway et al.[46], the value of b is as important as i_0 in characterising electrocatalysis. Consider, for example, the parameters presented for the non pre-treated Ni and Co anodes in Table 4. From the quoted steady state current density values, it is obvious that, at an overpotential of η = 0.302 V (which lies within the lower straight line Tafel regions in the polarisation curves for both anodes), it is the Ni electrode that displays the superior catalytic activity – yet it is the Co electrode that has the higher i_0 value. This arises due to the larger value of b in the case of the Co anode. This leads to the general conclusion, that where different electrodes present significantly different Tafel slopes for a given reaction, a comparison of the exchange current densities is not a

useful exercise [47, 48], if one is interested in the relative catalytic abilities of the electrodes at practically useful rates of reaction.

An alternative approach, and that utilised in the present work, is to compare the values of active surface area normalised (or "real") steady state current densities at a given overpotential. It has been elected to conduct such comparisons at an overpotential of η = 0.302 V. This overpotential was selected because it facilitates ready comparison of the real current densities observed at Ni, Co and Fe electrodes in the present work, with those observed by Bockris and Otagawa [47] for nickelate, cobaltate and ferrite electrodes at η = 0.3 V. The latter authors have described this low overpotential section of the Tafel region as being the practically important region for comparison.

Table 4. Comparison, based on the data of Fig. 17, of various parameters related to the OER catalytic activity of fresh non-electrochemically pre-treated Ni, Co and Fe electrodes in 1.0 M NaOH at 25°C. The quoted current densities are based on the estimated active surface areas for the OER of each electrode.

Electrode	f_r	b (mV dec^{-1})	i_0 (A cm^{-2})	i(0.302 V) (A cm^{-2})
Ni	7.3 ± 0.1	37.5	2.75 (±.04) ×10^{-13}	3.34 (± 0.05) × 10^{-5}
Co	13.1 ± 0.5	46.0	3.2 (±0.1) ×10^{-12}	1.15 (± 0.04) × 10^{-5}
Fe	0.52 ± .02	37.0	6.1 (±0.2) ×10^{-15}	9.5 (±0.4) ×10^{-7} [a]

[a] Estimated by the extrapolation of the lower overpotential Tafel slope line.

Table 5. Comparison, based on the data of Fig. 18, of various parameters related to the OER catalytic activity of pre-reduced Ni, Co and Fe electrodes in 1.0 M NaOH at 25°C. The quoted current densities are based on the estimated active surface areas for the OER of each electrode.

Electrode	f_r	b (mV dec^{-1})	i_0 (A cm^{-2})	i(0.302 V) (A cm^{-2})
Ni	6.3 ± 0.2	38.5	1.78 (±.07) ×10^{-13}	1.21 (± 0.04) × 10^{-5}
Co	12.9 ± 0.7	47.5	3.3 (±0.2) ×10^{-12}	7.4 (± 0.4) × 10^{-6}
Fe	0.51 ± .02	39.5	2.9 (±0.2) ×10^{-14}	1.3 (± 0.1) × 10^{-6} [a]

[a] Estimated by the extrapolation of the lower overpotential Tafel slope line.

Miles et al.[48] used what they called the Tafel parameter, a (a = -$b$log i_0 and is thus the experimental overpotential at a steady state current density of 1 A cm^{-2}), to compare the catalytic

activities for the OER, of thermally prepared electrodeposited oxides of various metals, in 30 wt% KOH solutions (~ 5.35 M) at 80ºC. They reported the following activity series; Ru >Ir~Pt~Rh~Pd~Ni~Os>>Co>>Fe. Their analysis however, suffers from the drawback of the reported current densities being referred to geometric surface areas and not to estimated real active surface areas.

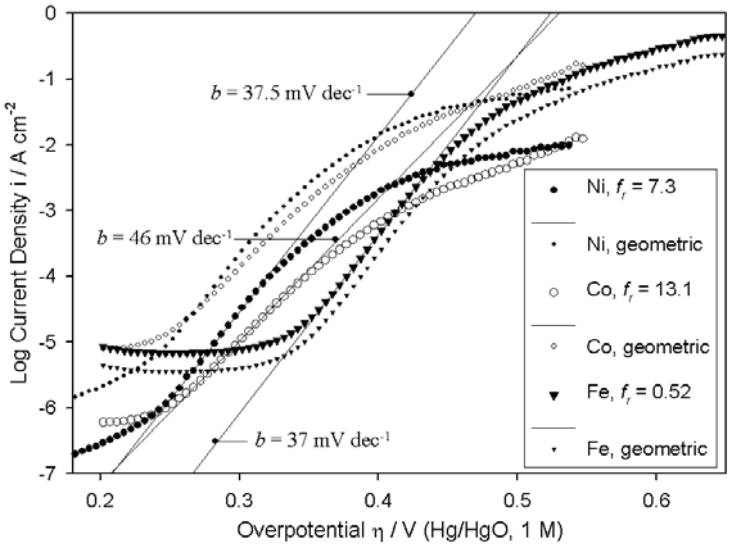

Figure 17. Comparison of *iR* corrected steady state polarisation curves recorded in 1.0 M NaOH solution at 25°C, for freshly prepared non-electrochemically pre-treated Ni, Co and Fe electrodes. As indicated in the legend each curve is presented for both the case where the current density values are based on the geometric electrode surface area and also the case where they have been normalised to the estimated active surface area.

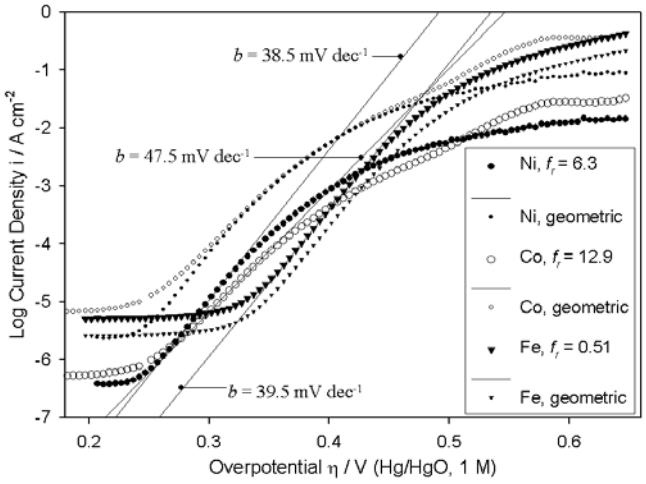

Figure 18. Comparison of *iR* corrected steady state polarisation curves recorded in 1.0 M NaOH solution at 25°C, for pre-reduced Ni, Co and Fe electrodes. As indicated in the legend each curve is presented for both the case where the current density values are based on the geometric electrode surface area and also the case where they have been normalised to the estimated active surface area.

As mentioned in the introduction, Scarr [5] conducted what was, until the present work, the only comparative study on the catalytic performance of polycrystalline Ni, Co and Fe electrodes towards the OER in alkaline solution. This worker observed Tafel slopes of $b = \sim 2.303 \times 4RT/5F$ for each of the three metals in 1 M KOH, thereby rendering meaningful a comparison of catalytic activities based on the relative values of the exchange current densities. In agreement with the trend reported by Miles et al.[48], values of $i_0 = 2 \times 10^{-10}$ A cm^{-2}, $i_0 = 8 \times 10^{-11}$ A cm^{-2} and $i_0 = 2 \times 10^{-13}$ A cm^{-2} were observed by Scarr for the Ni, Co and Fe anodes respectively. Unfortunately, the reported i_0 values were again normalised to the geometric surface area.

Examination of Figs. 17 and 18, and the associated Tables 4 and 5, reveals that, for $\eta \leq 0.4$ V (i.e. the range of overpotentials associated with the entire length of the lower *b* straight line regions for the Ni and Co electrodes, and most of the length of this region for the Fe electrodes), the real surface area normalised steady state polarisation curves of the present work are indicative of the same OER catalytic activity series as observed by Miles et al.[48] and Scarr [5] – i.e. Ni > Co > Fe. The data presented in these figures also indicates that the degree of inferiority of the catalytic activity of the Fe electrodes, relative to the Co and Ni electrodes, is overstated by steady state polarisation curves based on geometric surface areas, at least in the case of the polycrystalline metallic electrodes utilised here. This arises of course, due to the fact that roughness factors of less than unity have been estimated, via the OH_{ads} desorption method, for the Fe electrodes, in comparison with factors significantly larger than unity yielded by the same technique for the Ni [1] and Co [2] electrodes. Indeed in the case of the pre-reduced electrodes (Fig. 18), at overpotentials in the approximate range of $0.25 \text{ V} \leq \eta \leq 0.32$ V, the steady state polarization curves normalized to the geometric surface area, indicate that the Co electrode is catalytically superior to the Ni electrode. However, normalisation of these data to the respective values of the active surface area, reveals that the aforementioned apparent conclusion is actually incorrect.

Bockris and Otagawa [47] have reported the following OER steady state current density values, for various perovskite electrodes in 1.0 M NaOH (25°C) at $\eta = 0.3$V: $i = 1.3 \times 10^{-5}$ A cm^{-2} for a nickelate electrode ($f_r = 5.6 \times 10^3$) , $i = 1.4 \times 10^{-6}$ - 1.0×10^{-5} A cm^{-2} for various cobaltate anodes (f_r values of the order of $10^2 - 10^3$), $i = 5.0 \times 10^{-7}$ A cm^{-2} ($f_r = 6.0 \times 10^2$) for a $La_{0.7}Sr_{0.3}FeO_3$ ferrite electrode, and $i = 8.1 \times 10^{-7}$ A cm^{-2} ($f_r = 3.3 \times 10^3$) for a for a $La_{0.5}Sr_{0.5}FeO_3$ ferrite electrode. The quoted roughness factor values were estimated using the double layer capacitance ratio approach in conjunction with cyclic voltammetry measurements. Comparing the values of $i_{(\eta = 0.3\text{V})}$ obtained by Bockris and Otagawa [47] for their perovskite electrodes with the values of $i_{(\eta = 0.303\text{V})}$ observed in the present work and listed in Tables 4 and 5, it is apparent that there is agreement to within an order of magnitude between the values quoted for our oxidised polycrystalline metal electrodes and the perovskite electrodes (based on the corresponding transition metal) of the former authors. This order of magnitude agreement prevails despite the fact that the roughness factors of the perovskite electrodes are 2 – 3 orders of magnitude greater than the roughness factors of our electrodes. It might therefore be suggested that the OER occurs at *essentially the same type of active site* on an anodic oxide covered metal electrode surface, as on the corresponding perovskite electrode surface.

In his review on the OER, Kinoshita [10] commented that electrodes consisting of specifically pre-synthesised metal oxides (like the peroskite electrodes of Bockris and Otagawa [9, 47]) generally

display superior catalytic properties towards the reaction, compared to (anodic oxide covered) metallic electrodes. However, most literature reports on the OER do not attempt to normalise observed steady state current densities to estimated real surface areas. With this point in mind, and considering the conclusions of the previous paragraph, it might be suggested, that the apparently superior OER performance of synthesised metal oxide electrodes, relative to the oxide formed anodically on polycrystalline electrodes of the same metal, arises principally due to the larger available active specific surface areas of the former type of anode, and not due to any intrinsically superior electrocatalytic properties of the synthesised oxides.

The concept of a volcano plot is often encountered in attempts to rationalise the relative electrocatalytic activities for a given reaction, of different electrode materials, in terms of a given physicochemical property [49]. Attempts to draw correlations between electrode physicochemical properties and OER catalytic performance is complicated by the fact that it is the metal oxide and not metal that catalyses oxygen evolution. Kinoshita [10] has reviewed the efforts of various workers who have tackled this problem and sought to formulate a coherant theory of electrocatalysis for the OER. Amongst these, perhaps the most complete and successful attempt to provide an interpretation of OER catalytic activity in terms of physicochemical parameters was provided by Bockris and Otagawa [47] in their study of the reaction at perovskite electrodes. For perovskites based on the first row transition metal M (general formula AMO_3, where A is a lanthanide), they found that there was an inverse linear relationship between the estimated M(III)-OH bond strength and $i_{(\eta = 0.3V)}$ – i.e. while the estimated bond strength increases in the order Ni < Co < Fe < Mn < Cr, the OER catalytic activity follows the reverse of this series. They rationalised this in terms of a rate determining step involving the desorption of the OH_{ads} species adsorbed in the initial discharge step – obviously the weaker the M-OH bond the greater the rate of desorption at a given overpotential. Bockris and Otagawa devised molecular orbital diagrams for the bonding of an OH entity to a $M(III)O_5$ species (which they proposed as a valid model for a transition metal site in the {001} plane of the perovskite unit cell) and concluded that the M-OH bond strength had an inverse dependence on the number of d electrons occupying antibonding orbitals (4 for Ni(III)-OH, 3 for Co(III)-OH etc).

While at first glance, the aforementioned concepts of Bockris and Otagawa would appear to be in accord with our experimental observation of an OER activity series of Ni > Co > Fe at overpotentials associated with a (deduced) rate determining OH desorption step, some caution is in order. The relationship between M-OH bond strength and OER catalytic activity, and the molecular orbital analysis referred to above, apply specifically to first row transition metal ions in the +3 oxidation state. While this is consistent with the RDS of the pathway that we have proposed for the OER at oxidised Ni substrates [1], it is clearly not the case for the RDS envisaged in the present article (step (B II)), in which an Fe(VI)-OH chemical bond is broken. Similarly in the case of Co, it is our contention that the rate limiting OH desorption step involves the breaking of a Co(IV)-OH rather than a Co(III)-OH bond. Nevertheless, if it is the case that the molecular orbital electron configurations for the Co(IV)-OH and Fe(IV)-OH bonds are the same as those proposed by Bockris and Otagawa[47] (see Figs. 14 and 20 in that reference) for Fe(III)-OH and V(III)-OH respectively, then the correlation envisaged by the same authors between the number of d electrons in antibonding orbitals and OER catalytic activity would also hold for the electrodes of the present work, based on rate determining

steps involving the breaking of Ni(III)-OH (4 antibonding electrons), Co(IV)-OH (2 antibonding electrons) and Fe(IV)-OH (1 antibonding electon) bonds. In conclusion we comment that our observation of similar (real surface area normalised) OER catalytic activities at passive oxide covered Co (catalytic site envisaged to be in the Co(IV) valance state) and Fe (catalytic site envisaged to be in the Fe(VI) valance state) electrodes, to those observed by Bockris and Otagawa [47] at their cobaltate and ferrite electrodes, may cast some doubt on the conviction of these authors (based on rather little experimental evidence) that M(III) sites are the OER active centres at the surface of electrodes of all perovskites. If this assumption regarding the common valance state of the catalytic ions at perovskite surfaces is not true, then the correlation of OER activity with the number of antibonding d-electrons becomes more complicated than that originally envisaged by Bockris [47](although it might well still be applicable).

4. CONCLUSIONS

We now summarise the principal conclusions arising from our entire three article treatment of the OER at anodic oxide covered Ni, Co and Fe electrodes in aqueous alkaline solution.

Firstly, a common theme throughout this series of articles has been the observation that the nature of electrode pre-treatment and the degree of ageing can have a significant effect on the experimentally measured kinetic parameters. Pre-treatment routines (particularly cathodic pre-reduction followed by a single voltammetric cycle between the hydrogen and oxygen evolution regions of potential) have been found to be necessary in obtaining consistent data sets with meaningful values of the Tafel slope, b, and the OH^- ion reaction order, m_{OH^-}.

The sole pathway, that can account for the entire set of experimental parameters observed for the various Co and Fe electrodes, is the *physisorbed hydrogen peroxide mechanism*, presented in the present paper, for Fe, as scheme (B). The second step of this pathway, which involves the breaking of a M-OH chemical bond, is considered to be rate limiting. The different values of b and m_{OH^-} observed for electrodes subjected to different pre-treatments, or for the same electrode at different overpotentials, arise due to changes in the fractional coverage θ of the reaction intermediates, and not due to changes in rate determining step.

A similar mechanistic pathway is likely to prevail for oxidised Ni anodes, except that the OH^- ion that reacts in the rate determining second step originates from the surface anionic complex $[Ni(III)O_m(OH)_{n+1}]^{p-}$ (p=2m+n-3) rather than from the bulk solution [1]. An alternative pathway involving the cyclical formation and decomposition of an unstable Ni(IV) entity cannot be ruled out on the basis of the experimental data. However a change in the catalytic metal ion oxidation state is not suggested by the data obtained for Co and Fe electrodes, and thus in the greater scheme of things, the Ni(III) physisorbed peroxide pathway would seem to be the most consistent solution to the problem of mechanistic determination for the OER at passive oxide covered Ni anodes. Unlike the Ni(IV) path, the RDS for the Ni(III) scheme involves the desorption of a chemisorbed OH entity, which is consistent with the possibly applicable OER electrocatalytic theory of Bockris and Otagawa, as discussed in the previous section.

In the previous paragraph we referred to the anionic surface complex which we have postulated to be the active site for the OER on oxidised Ni substrates. In general we have found that, giving consideration to the acidic nature of hydrated oxide surfaces at high pH, is extremely useful in understanding the OER at such surfaces in aqueous alkaline media. Since in general, the catalytic centres for oxygen evolution reside on the surface of an oxide phase in contact with aqueous solution, the surface region of the oxide will inevitably become somewhat hydrated. In view of this, it is our belief that all workers in this area should consider the amphoteric nature of their oxide surfaces, regardless of how the oxide phase was prepared. It is, for example, to take the case of a Ni anode in alkaline solution[1], more realistic to represent the OER active site as $[Ni(III)O_m(OH)_n]^{p-}$ (where extra hydroxide ions have been coordinated from solution, owing to the acidic nature of the oxide in electrolytes of high pH), rather than the traditional practice of considering it to be a discrete NiOOH entity.

The observation, under particular circumstances, of Tafel slopes of 45 – 48 mV dec^{-1} ($b \cong 2.303(4RT/3F)$ at 25ºC) or ca. 240 mV dec^{-1} ($b \cong 2.303(4RT/F)$ at 25ºC) for passive oxide covered Fe and Co [2] electrodes has been explained in terms of the existance of a second potential barrier, related to the field driven migration of charge carriers across the oxide layer, in series with the normal electrochemical charge transfer barrier at the oxide surface/solution interface. This model was devised many years ago – our new contribution has been to identify the "barrier layer" with the inner compact anhydrous region of the passive oxide film.

On the basis of electrochemical impedance spectroscopy (EIS) measurements, we have modelled in terms of equivalent circuits, the complex metal/oxide/solution interface for each of the three metals, at overpotentials associated with significant OER current density. For Ni and Fe electrodes, the ac measurements confirmed the OER kinetic parameters obtained by the conventional dc steady state polarisation approach – in the case of Co in 1.0 M NaOH, a large low frequency pseudo-capacitive contribition probably arising from the surface Co(III)↔Co(IV) redox transition, rendered impractical the extraction of OER kinetic parameters from EIS data [2].

Normalisation of experimental $i(\eta)$ characteristics to estimated electrode active surface areas revealed an activity series for the OER (in terms of decreasing activity in the lower Tafel slope region of potential) of Ni > Co > Fe. As discussed in the previous section, this observation aligned with the fact that we envisage the RDS for all electrodes studied to involve the desorption of an OH entity, suggests that our experimental data conforms to the electrocatalytic theory of the OER devised by Bockris and Otagawa [47]. However we envisage that the central metal ion of the electrocatalytically active surface complexes exist in the Ni(III), Co(IV) and Fe(VI) valance states for oxidised Ni, Co and Fe anodes respectively, and not in a common oxidation state as was proposed by Bockris for perovskite electrodes based on these (and other first row transition metal) elements. In view of this, it is our conclusion that while the relatively simple model of Bockris and Otagawa [47] captures the essence of the dependence of OER activity on the transition metal of the anode oxide material, a further layer of sophistication is required to account for the fact that the oxidation state of the active metal ion probably varies from the oxide of one element to another (within the same periodic table row).

ACKNOWLEDGEMENT
The authors are grateful for the financial support of Enterprise Ireland Grant Number SC/2003/0049, IRCSET Grant Number SC/2002/0169 and the HEA-PRTLI Program.

References

1. M.E.G. Lyons, M.P. Brandon, *Int. J. Electrochem. Sci.,* 3(2008) 1386
2. M.E.G. Lyons, M.P. Brandon, *Int. J. Electrochem. Sci.,* 3(2008) 1425
3. M.E.G. Lyons ,L.D. Burke, *J. Electroanal. Chem*., 170(1984) 377.
4. M.E.G. Lyons, M.P. Brandon, *Phys. Chem. Chem. Phys.,* 2008, submitted for publication. Paper number: B815338H.
5. R.F. Scarr, *J. Electrochem. Soc.*, 116(1969) 1526.
6. A.I. Krasil'shchikov, *Zh. Fiz. Khim.*, 37(1963) 531.
7. R. Šimpraga and B.E. Conway, *J. Electroanal. Chem.*, 313(1991) 161.
8. M.E.G. Lyons , L.D. Burke, *J. Electroanal. Chem*., 198(1986) 347.
9. J.O'M. Bockris and T. Otagawa, *J. Phys. Chem.*, 87(1983) 2960.
10. K. Kinoshita, *Electrochemical Oxygen Technology*, Wiley-Interscience, New York, 1992, chapter 2, pp. 78-99.
11. A. Damjanovic, A. Dey and J.O'M. Bockris, *Electrochim. Acta.*, 11(1966) 791.
12. J.C.K. Ho and D.L. Piron, *J. Appl. Electrochem.*, 26(1996) 515.
13. R.A. Robinson and R.H. Stokes, *Electrolyte Solutions*, Revised 2nd Edition, Butterworth & Co. Ltd., London, 1965, p. 492.
14. H. Willems, A.G.C. Kobussen, J.H.W. De Wit and G.H.J. Broers, *J. Electroanal. Chem*, 170(1984) 227.
15. M.R. Gennero De Chialvo, A.C. Chialvo, *Electrochim. Acta*, 35(1990) 437.
16. R.N. Singh, J.P. Singh, B. Lal, M.J.K Thomas and S. Bera, *Electrochim Acta*, 51(2006) 5515.
17. D.D. MacDonald and B. Roberts, *Electrochim. Acta.*, 23(1978) 557.
18. R.S.S. Guzman, J.R. Vilche and A.J. Arvia, *Electrochim. Acta*, 24(1979) 395.
19. S. Juanto, R.S.S. Guzman, J.O. Zerbino, J.R. Vilche and A.J. Arvia, *Electrochim. Acta*, 36(1991) 1143.
20. J. Flis, H. Oranowska , Z. Szklarska-Smialowska, *Corros. Sci.*, 30(1990) 1085.
21. S.T. Amaral, E.M.A. Martini and I.L. Muller, *Corros. Sci.*, 43(2001) 853.
22. G. Larramona ,C. Gutierrez, *J. Electrochem. Soc.*, 136(1989) 2171.
23. S. Joiret, M. Keddam, X.R. Novoa, M.C. Perez, C. Rangel and H. Takenouti, *Cement & Concrete Composites*, 24(2002) 7.
24. L.D. Burke and M.E.G. Lyons, in *Modern Aspects of Electrochemistry, Vol. 18*, R.E. White, J.O'M. Bockris and B.E. Conway, Eds., Plenum Press, New York, 1986, p169.
25. L.D. Burke and E.J.M. O'Sullivan, *J. Electroanal. Chem.*, 117(1981) 155.
26. L.D. Burke and D.P. Whelan, *J. Electroanal. Chem.*, 162(1984) 121.
27. L.D. Burke, M.I. Casey, V.J. Cunnane, O.J. Murphy and T.A.M. Twomey, *J. Electroanal. Chem.*, 189(1985) 353.
28. A.G.C. Kobussen and C.M.A.M. Mesters, *J. Electroanal. Chem.*, 115(1980) 131.
29. A.G.C. Kobussen, H. Willems and G.H.J. Broers, *J. Electroanal. Chem.*, 142(1982) 85.
30. A. Damjanovic and B. Jovanovic, *J. Electrochem. Soc.*, 123 (1976) 374.
31. V. I. Birss, A. Damjanovic and P.G. Hudson, *J. Electrochem. Soc.*, 133(1986) 1621.
32. V. I. Birss and A. Damjanovic, *J. Electrochem. Soc.*, 134(1987) 113.
33. M.E.G. Lyons, M.P. Brandon, J. Electroanal. Chem., in preparation.
34. D.A. Harrington and B.E. Conway, *Electrochim. Acta.*, 32(1987) 1703.

35. B.E. Conway, in *Impedance Spectroscopy – Theory, Experiment, and Applications*, 2nd Edition, E. Barsoukov and J.R. Macdonald, Ed., J. Wiley & Sons, 2005, section 4.5.3.,, pp.469-497.
36. R.E. Meyer, *J. Electrochem. Soc.*, 107(1960) 847.
37. J.J. MacDonald , B.E. Conway, *Proc. R. Soc. London, Ser. A*, 269(1962) 419.
38. S. Trasatti , O.A. Petrii, *Pure & Appl. Chem*., 63(1991) 711.
39. A.I. Fedorova , A.N. Frumkin, *J. Phys. Chem. USSR*, 27(1953) 247.
40. B. Beverskog , I. Puigdomenech, *Corros. Sci.*., 38(1996) 2121.
41. K Bouzek and I. Rousar, *J. Appl. Electrochem.*, 23(1993) 13.
42. K Bouzek and I. Rousar, *J. Appl. Electrochem.*, 23(1993) 919.
43. A.N. Frumkin, P. Dolin and B.V. Ershler, *Acta Physiochim., U.R.S.S.*, 13(1940) 747 ; 802.
44. L. Bai, D.A. Harrington and B.E. Conway, *Electrochim. Acta*, 32(1987) 1713.
45. N. Krstajic, M. Popovic, B. Grgur, M. Vojnovic and D. Sepa, *J. Electroanal. Chem*., 512(2001) 16.
46. B.E. Conway, L. Bai and M.A. Satter, *Int. J. Hydrogen Energy*, 12(1987) 607.
47. J.O'M. Bockris and T. Otagawa, *J. Electrochem. Soc.*, 131(1984) 290.
48. M.H. Miles, Y.H. Huang and S. Srinivasan, *J. Electrochem. Soc.*, 125(1978) 1931.
49. S Trasatti in *Handbook of Fuel Cells, Fundamentals Technology and Applications, Vol 2, Electrocatalysis*, W. Vielstich, A. Lamm and H.A. Gasteiger, Eds., John Wiley and Sons, Chichester, 2003, chapter 10.